



# CHORUS

This is the accepted manuscript made available via CHORUS. The article has been published as:

## Signature of the fragmentation of a color flux tube

Cheuk-Yin Wong

Phys. Rev. D **92**, 074007 — Published 7 October 2015

DOI: [10.1103/PhysRevD.92.074007](https://doi.org/10.1103/PhysRevD.92.074007)

# The Signature of the Fragmentation of a Color Flux Tube

Cheuk-Yin Wong<sup>1,\*</sup>

<sup>1</sup>*Physics Division, Oak Ridge National Laboratory, Oak Ridge, Tennessee 37831, USA*

The production of quark-antiquark pairs along a color flux tube precedes the fragmentation of the tube. Because of local conservation laws, the production of a  $q\bar{q}$  pair will lead to correlations of adjacently produced mesons (mostly pions). Adjacently produced mesons however can be signalled by their rapidity difference  $\Delta y$  falling within the window of  $|\Delta y| \lesssim 1/(dN/dy)$ , on account of the space-time-rapidity ordering of produced mesons in a flux tube fragmentation. Therefore, the local conservation laws of momentum, charge, and flavor will lead to a suppression of angular correlation function  $dN/(d\Delta\phi d\Delta y)$  for two mesons with opposite charges or strangeness on the near side at  $(\Delta\phi, \Delta y) \sim 0$ , but an enhanced correlation on the back-to-back, away side at  $\Delta\phi \sim \pi$ , within the window of  $|\Delta y| \lesssim 1/(dN/dy)$ . These properties can be used as signatures for the fragmentation of a color flux tube. The gross features of the signature of flux tube fragmentation for two oppositely charged mesons are qualitatively consistent with the STAR and NA61/SHINE angular correlation data for two hadrons with opposite charges in the low- $p_T$  region in high-energy  $pp$  collisions.

PACS numbers: 13.86.Hd, 13.66.Bc

## I. INTRODUCTION

In the production of particles in the central rapidity region in high-energy hadron-hadron collisions and  $e^+e^-$  annihilations, the low- $p_T$  part of the spectra falls within the realm of soft nonperturbative QCD physics and is usually considered to arise from the fragmentation of a color flux tube (or its idealization as a QCD string) [1–9, 11–20]. The high- $p_T$  part in hadron-hadron collisions is considered to arise from a relativistic hard scattering of partons and subsequent parton showering [10, 20–34]. In the case of high-energy  $e^+e^-$  annihilation, the annihilation leads to the production of high-energy quark and antiquark partons which are then subject to perturbative QCD parton showering processes to lead to the production of hadrons.

Recently, it was found that the hadron  $p_T$  spectra spanning over 14 decades of magnitude from about 0.5 GeV/c to the highest  $p_T$  at central rapidity in  $pp$  collisions at LHC energies can be adequately described by a Tsallis distribution with only three degrees of freedom [32–38], in a form phenomenologically equivalent to the quasi-power law introduced by Hagedorn [39] and others [40] for relativistic hard scattering. The simplicity of the  $p_T$  spectrum suggests that a single mechanism dominates over the domain with  $p_T > 0.5$  GeV/c at central rapidity in these high energy collisions. As the high- $p_T$  region is known to arise from the relativistic hard-scattering process [10, 20–34], one is led to the suggestion that the hard-scattering process dominates over the domain with  $p_T > 0.5$  GeV/c in these high-energy  $pp$  collisions. Additional experimental evidences have been uncovered to support such a suggestion [38].

The dominance of the hard scattering process does not imply the absence of the soft flux tube fragmentation process. It only stipulates that contributions from

the hard-scattering process increase with increasing collision energies and the fraction of the contributions from the flux tube fragmentation process becomes smaller in comparison, as pointed out earlier in [28, 29]. As a consequence, there will be a transverse momentum boundary  $p_{Tb}$  which separates the lower domain of flux tube fragmentation from the higher domain of hard scattering dominance.

As the  $pp$  collision energy decreases, the role of the flux-tube fragmentation and hard-scattering will be reversed, with an increase in the fraction of contributions from the flux-tube fragmentation and a shift of the transverse momentum boundary  $p_{Tb}$  to greater  $p_T$  values. It is of interest to see how the two processes interplay and how the boundary function  $p_{Tb}(\sqrt{s_{NN}})$  between the two processes depends on the collision energy  $\sqrt{s_{NN}}$ . In addition to being an intrinsic physical property of the  $pp$  collision process, the boundary function  $p_{Tb}(\sqrt{s_{NN}})$  separating the two processes in  $pp$  collisions may have implications on the early evolution dynamics, the thermalization of the produced medium, the quenching of jets, and the formation of the quark-gluon plasma, in high-energy nucleus-nucleus collisions. It is therefore desirable to search for ways to discriminate the process of flux tube fragmentation from the process of the hard scattering in  $pp$  collisions so that they can be separated out and the boundary  $p_{Tb}$  mapped out as a function of the collision energy. We need well-defined signatures for the flux tube fragmentation and the hard-scattering processes.

Two-hadron  $\Delta\phi$ - $\Delta\eta$  angular correlations have been previously suggested and used by the STAR Collaboration to separate phenomenologically the ‘soft’ and ‘hard’ components in nucleon-nucleon and nucleus-nucleus collisions [41–45]. The signature for the hard component, represented by the production of two back-to-back jets (minijets) in the hard-scattering process, is well-known [10, 23–27, 30], as indicated for example by STAR  $\Delta\phi$ - $\Delta\eta$  correlation data for two oppositely-charged hadrons with  $p_T > 0.5$  GeV/c in  $pp$  collisions at  $\sqrt{s_{NN}} = 200$  GeV

\* wongc@ornl.gov

shown in Fig. 1(b) [41–45]. It consists of (i) a near-side cluster of particles at  $(\Delta\phi, \Delta\eta)\sim 0$  for one jet, and (ii) an away-side ridge at  $\Delta\phi\sim\pi$  along  $\Delta\eta$  for the other jet.

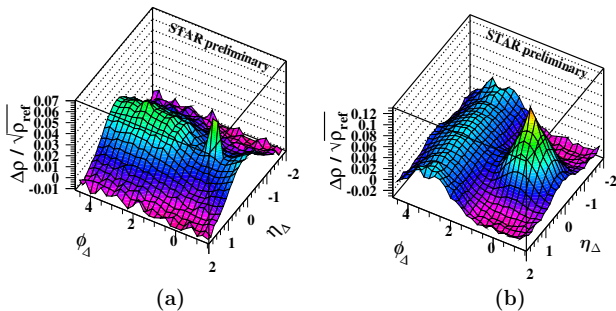


FIG. 1. (Color online) The angular correlation data  $\Delta\rho/\sqrt{\rho_{\text{ref}}}$  as a function of the azimuthal angle difference  $\phi_{\Delta}=\Delta\phi$  and pseudorapidity difference  $\eta_{\Delta}=\Delta\eta$  of two oppositely-charged hadrons in  $pp$  collisions at  $\sqrt{s_{NN}}=200$  GeV (from Fig. 3 of [42] of the STAR Collaboration). Fig. 1(a) is for hadrons in the domain with  $p_T<0.5$  GeV/c and Fig. 1(b) for hadrons in the domain with  $p_T>0.5$  GeV/c

On the other hand, the ‘soft’ component, defined phenomenologically by the STAR Collaboration to be the mechanism that dominates the production process in the domain with  $p_T<0.5$  GeV/c for  $pp$  collisions at  $\sqrt{s_{NN}}=200$  GeV, was associated with the  $(\Delta\phi, \Delta\eta)$  correlation for two oppositely-charged hadrons as shown in Fig. 1(a) [41–45]. The correlation is suppressed at  $(\Delta\phi, \Delta\eta)\sim 0$  but enhanced at  $(\Delta\phi\sim\pi, \Delta\eta\sim 0)$ . The two-hadron correlation of the soft component was also taken phenomenologically as a one-dimensional Gaussian distribution at  $\Delta\eta\sim 0$  independent of  $\Delta\phi$  [41–45]. A rigorous proof of the microscopic connection between the two-hadron  $\Delta\phi$ - $\Delta\eta$  correlation and the signature of flux tube fragmentation is still lacking. The other suggested signature of a one-dimensional Gaussian at  $\Delta\eta\sim 0$  also needs to be re-examined carefully. Starting from the constituent level, the microscopic connection of  $dN/(d\Delta\phi)(d\Delta\eta)$  in a flux tube fragmentation will be the subject of the present investigation.

The search for the signature of the fragmentation of the flux tube is also useful for a better understanding of the multiparticle dynamics of the fragmentation process. Experimental verification of the signature will pave the way for further investigations to find out how a leading quark and an antiquark pair can produce a chain of hadrons that are ordered in space-time and rapidities through the non-perturbative QCD processes. Of particular interest is the possibility of an event-by-event exclusive measurement in which all of the momenta of the produced particles in a reaction event are measured, matched, and correlated, as in a jigsaw puzzle, to see how the space-time-rapidity ordering may allow the event reconstruction of the chain of hadrons at the moment of flux tube fragmentation.

To search for the signature, we envisage that in a flux tube fragmentation in hadron-hadron collisions or  $e^+e^-$

annihilations, a flux tube is initially formed between the leading quark and antiquark (or diquark in the case of a nucleon-nucleon collision) when they pull apart from each other at high energies. The vacuum is so polarized that ordered pairs of quarks and antiquarks are produced inside the tube via the Schwinger pair production mechanism or the QED2 inside-outside cascade mechanism [1, 2, 4, 5, 13–18, 20]. The interaction of the produced quarks with anti-quarks produced in adjacent vertices lead to the production of mesons and the fragmentation of the flux tube.

The production of a quark-antiquark pair needs to obey local conservation laws. These conservation laws will impose constraints and will lead to correlations of various quantities, for two longitudinally-adjacent produced mesons. The occurrence of two longitudinally-adjacent produced mesons, on the other hand, is signalled by their proximity in rapidity, on account of the space-time-rapidity ordering of the produced mesons (see for example, Chapter 6 of [20]). Hence, the local conservation laws will lead to correlations of various quantities as a function of the azimuthal angle difference  $\Delta\phi$  and rapidity difference  $\Delta y$  (or approximately, the pseudorapidity difference  $\Delta\eta$ ) for a pair of produced mesons in a flux tube fragmentation. These angular correlations can be used as the signature of the flux tube fragmentation in high-energy nucleon-nucleon collisions and  $e^+e^-$  annihilations.

In this paper, we restrict our attention to the central rapidity region. In Section II, for a system of four produced constituents we single out the relevant degrees of freedom to describe the flux tube fragmentation process. In Section III, we discuss the momentum distribution of two non-adjacent mesons when the quark and antiquark constituents in the detected mesons are produced without correlations. In Section IV, we examine the transverse momentum distribution of adjacent mesons in which the quark of one meson and the antiquark of the other meson are produced at the same point, subject to local conservation of momentum. In Section V, we discuss the rapidity distribution of produced mesons in a flux tube. In Section VI, we examine the charge correlation of two adjacent and non-adjacent mesons for a system with two flavors. In Section VII, we consider the correlation of charge and strangeness for two adjacent and non-adjacent mesons for a system with three flavors. In Section VIII, we present the two-particle correlation function for measurements with different combinations of meson charges and strangeness quantum numbers. In Section IX, we present numerical examples of theoretical correlation functions of  $dN/d\Delta\phi d\Delta\eta$  for different charge and strangeness configurations to provide signatures for flux tube fragmentation. In Section X, we compare the theoretical signature of the correlation of two oppositely charged hadrons with STAR and NA61/SHINE two-hadron correlation data for  $pp$  collisions [41–44, 46–49]. In Section XI, we present our conclusions and discussions.

## II. PRODUCTION OF TWO MESONS IN FLUX TUBE FRAGMENTATION

Our objective is to search for the signature of flux tube fragmentation by studying the correlations between two mesons produced in a flux tube. Starting with the microscopic constituent momenta, it is necessary to enumerate the relevant degrees of freedom before we can examine the correlations of the observed composite mesons.

We consider the production of two adjacent mesons in a flux tube at the moment of its fragmentation, as depicted schematically in Fig. 2 where the leading quark pulls apart in one direction while the other leading antiquark pulls apart in the other direction at high energies. As the leading quark and antiquark pull apart, a flux tube is formed and the vacuum in the tube is polarized. The flux tube fragmentation process is initiated by the production of many ordered  $q\bar{q}$  pairs along the flux tube by the Schwinger particle production mechanism or the inside-outside cascade mechanism, as discussed in [1, 2, 4–9, 11–18, 20]. The production of these  $q\bar{q}$  pairs takes place locally at spatial points along the tube.

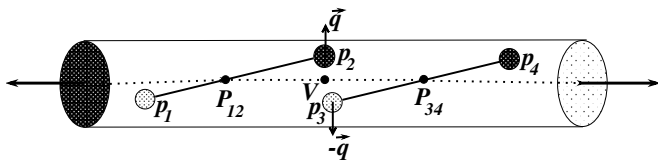


FIG. 2. Schematic depiction of the production of quarks and antiquarks in two adjacent mesons  $P_{12}$  and  $P_{34}$  as the leading quark is pulling to the left and the leading antiquark is pulling to the right, with the production of  $p_1$ (antiquark),  $p_2$ (quark),  $p_3$ (antiquark) and  $p_4$ (quark) along the flux tube. Subsequently  $p_1$  interacts with  $p_2$  to form meson  $P_{12}$ , while  $p_3$  interacts with  $p_4$  to form meson  $P_{34}$ .

We focus our attention in a small section in the central rapidity region in the center-of-mass system and consider the pair  $p_2$ (quark) and  $p_3$ (antiquark) produced at the vertex  $V$  in Fig. 2. We shall use the particle label also to represent the particle momentum. After  $p_2$  and  $p_3$  are produced,  $p_2$  interacts with the adjacent antiparticle  $p_1$  with a confining interaction, leading to the formation of the meson  $P_{12}$ . Similarly,  $p_3$  interacts with the adjacent  $p_4$  to form the adjacent meson  $P_{34}$ . In the leading order of the confining interaction, the constituents of meson  $P_{12}$  and the constituents of the adjacent meson  $P_{34}$  do not interact<sup>1</sup> because the linearly confining interactions are screened by their partners. The formation of the nearly non-interacting mesons  $P_{12}$  and  $P_{34}$  leads to the fragmentation of the flux tube into mesons along the longitudinal direction, populating the longitudinal momentum space in the form of a rapidity plateau.

<sup>1</sup> There are however higher-order residual interactions between mesons, as discussed for example in Peshkin and Bhanot [50] and [51, 52].

The pair-wise two-body interaction between  $p_1$  and  $p_2$  as well as between  $p_3$  and  $p_4$  along the flux tube makes it simple to study the many-body problem of quarks and antiquarks in two-body basis [52, 53]. We can use Dirac's constraint dynamics [53–59] to separate out the coordinates of a pair of particles into their center-of-mass and relative coordinates in a relativistically consistent manner.

For the pair of interacting particles with 4-momenta  $p_1$  and  $p_2$  and rest masses  $m_1$  and  $m_2$ , we construct the total momentum  $P_{12}$  and the relative momentum  $p_{12}$ ,

$$P_{12} = p_1 + p_2, \quad (1a)$$

$$p_{12} = \frac{p_2 \cdot P_{12}}{P_{12}^2} p_1 - \frac{p_1 \cdot P_{12}}{P_{12}^2} p_2, \quad (1b)$$

where

$$\frac{p_1 \cdot P_{12}}{P_{12}^2} = \frac{P_{12}^2 + p_1^2 - p_2^2}{2P_{12}^2} \quad (2a)$$

and

$$\frac{p_2 \cdot P_{12}}{P_{12}^2} = \frac{P_{12}^2 + p_2^2 - p_1^2}{2P_{12}^2} \quad (2b)$$

are the projections of the momenta  $p_1$  and  $p_2$  along the direction of the total momentum  $P_{12}$ . The inverse transformation is

$$p_1 = \frac{p_1 \cdot P_{12}}{P_{12}^2} P_{12} + p_{12}, \quad (3a)$$

$$p_2 = \frac{p_2 \cdot P_{12}}{P_{12}^2} P_{12} - p_{12}. \quad (3b)$$

Under the interaction  $\Phi(x_{\perp 12})$  which depends only on the time-transverse relative coordinate  $x_{\perp 12}$  between  $p_1$  at  $x_1$  and  $p_2$  at  $x_2$ , namely,

$$x_{\perp 12} = (x_1 - x_2) - \frac{(x_1 - x_2) \cdot P_{12}}{P_{12}^2} P_{12}, \quad (4)$$

with the property  $x_{\perp 12} \cdot P_{12} = 0$ , the eigenvalue equation for the meson bound state with wave function  $\psi(x_{\perp 12})$  in the relative coordinate is [53–59]

$$[b^2(P_{12}^2; m_1^2, m_2^2) + \boldsymbol{p}_{12}^2 - \Phi(x_{\perp 12})]|\psi(x_{\perp 12})\rangle = 0, \quad (5)$$

where

$$b^2(P_{12}^2, m_1^2, m_2^2) = \frac{P_{12}^4 - 2P_{12}^2(m_1^2 + m_2^2) + (m_1^2 - m_2^2)^2}{4P_{12}^2}, \quad (6)$$

$$P_{12}^2 = M_{12}^2, \quad (7)$$

and

$$M_{12} = \sqrt{b^2 + m_1^2} + \sqrt{b^2 + m_2^2}. \quad (8)$$

The solution of the bound state equation (5) then leads to the meson wave function  $\psi(x_{\perp 12})$  and the meson mass

$M_{12}$ .<sup>2</sup> Equations (5) and (7) indicate that as a result of the interaction  $\Phi(x_{\perp 12})$  that exists between  $p_1$  and  $p_2$ , the momentum elements are related by

$$dp_1\delta(p_1^2 - m_1^2)dp_2\delta(p_2^2 - m_2^2) \\ = dP_{12}\delta(P_{12}^2 - M_{12}^2)dp_{12}\delta(b^2 - \mathbf{p}_{12}^2 - \Phi(x_{\perp 12}))\delta(p_{0,12}). \quad (9)$$

In the context of the fragmentation of the a flux tube, the produced antiquark  $p_1$  and the quark  $p_2$  line up along the tube as in a one-dimensional string at the initial moment of meson production, and one can use the string approximation to separate out the longitudinal and transverse degrees of freedom by approximating the  $\mathbf{p}_{12}$  in Eq. (5) by  $p_{z12}$  and the confining potential coordinate  $x_{\perp 12}$  to be longitudinal. The longitudinal  $p_{z12}$  and the transverse degrees of freedom can then be separated. The solution of the bound state problem takes care of the  $p_{z12}$  degrees of freedom. Upon separating out and subsequently integrating over the variables of  $P_{0,12}$ ,  $p_{0,12}$  and  $p_{z,12}$ , the remain relevant degrees of freedom in the momentum element for particles  $p_1$  and  $p_2$  in the flux tube fragmentation are

$$\frac{dP_{z12}}{E_{12}}d\mathbf{P}_{T12}d\mathbf{p}_{T12} = dy_{12}d\mathbf{P}_{T12}d\mathbf{p}_{T12}, \quad (10)$$

where  $y_{12}$  is the rapidity of the meson  $P_{12}$ , and the subscripts  $T$  represent the transverse (2-dimensional) components.

Similarly, the particles  $p_3$  and  $p_4$  can be described by a composite meson with total momentum  $P_{34}$

$$P_{34} = p_3 + p_4, \quad (11a)$$

$$p_{34} = \frac{p_4 \cdot P_{34}}{P_{34}^2}p_3 - \frac{p_3 \cdot P_{34}}{P_{34}^2}p_4, \quad (11b)$$

with a relative momentum  $p_{34}$  containing a bound state with the meson mass  $P_{34}^2 = M_{34}^2$ . The inverse transformation is

$$p_3 = \frac{p_3 \cdot P_{34}}{P_{34}^2}P_{34} + p_{34}, \quad (12a)$$

$$p_4 = \frac{p_4 \cdot P_{34}}{P_{34}^2}P_{34} - p_{34}. \quad (12b)$$

The relevant degrees of freedom in the momentum element for particles  $p_3$  and  $p_4$  in the flux tube fragmentation are

$$dy_{34}d\mathbf{P}_{T34}d\mathbf{p}_{T34}. \quad (13)$$

Thus, for two mesons  $P_{12}$  and  $P_{34}$  in the problem of flux tube fragmentation, the probability distribution  $dN$  is in general a function of  $dN(y_{12}, y_{34}, \mathbf{P}_{T12}, \mathbf{P}_{T34}, \mathbf{p}_{T12}, \mathbf{p}_{T34})$ .

<sup>2</sup> In practice, the quark and antiquark have spins, and one needs to use the two-body Dirac equation in place of Eq. (5) for the eigenvalue equation involving a color-Coulomb plus a linear confining interaction. The numerical solution of the relativistic two-body Dirac equation then leads to the meson state with the meson mass  $M_{12}$  and the proper meson spatial wave function, as described in [60, 61] and references cited therein. A non-relativistic model of a meson as a  $q\bar{q}$  bound state is given in [62, 63].

### III. THE TWO-PARTICLE TRANSVERSE DISTRIBUTION FOR NON-ADJACENTLY PRODUCED MESONS

The process of  $q\bar{q}$  production for two adjacent mesons  $P_{12}$  and  $P_{34}$  depicted in Fig. 2 occurs in the neighborhood of the vertex  $V$ . We envisage that similar processes of  $q\bar{q}$  production occur independently at many other vertices along the flux tube, leading to the production of mesons populating the longitudinal momentum space in the form of a rapidity plateau.

We can consider two of the produced mesons which can be related to each other in two different ways. The mesons  $P_{12}$ , and  $P_{34}$  can be in a (longitudinally) adjacent state as in Fig. 2, in which the quark  $p_2$  of  $P_{12}$  and the antiquark  $p_3$  of  $P_{34}$  are produced at the same spatial point  $V$  and are correlated. The two mesons  $P_{12}$ , and  $P_{34}$  can be in a (longitudinally) non-adjacent state as in Fig. 3, in which all quarks and the antiquarks of the two mesons are independently produced at different vertices and are not correlated with each other. We shall often label the state of two mesons by the superscript  $X$  with  $X=A$  for the adjacent state and  $X=N$  for the non-adjacent state.

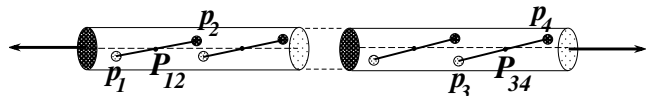


FIG. 3. Schematic depiction of the production of quarks and antiquarks  $p_1$ ,  $p_2$ ,  $p_3$ , and  $p_4$  in two non-adjacent mesons  $P_{12}$  and  $P_{34}$ , in a flux tube fragmentation. The quark  $p_2$  and the antiquark  $p_3$  are not correlated because they are produced at different vertices.

In the production of the four constituents  $p_1, p_2, p_3, p_4$ , we can separate out the longitudinal and transverse degrees of freedom to write the distribution as

$$dN = dN_y dN_T. \quad (14)$$

The probability for the two-meson state to be adjacent or non-adjacent depends mainly on the magnitude of their longitudinal rapidity differences  $|\Delta y|$  in comparison with the inverse of the rapidity density,  $1/(dN/dy)$ , which we shall take up in Section V. We examine in this section the transverse momentum distribution of non-adjacent meson,  $dN_T^N$ , and in the next section the the transverse momentum distribution of adjacent mesons,  $dN_T^A$ .

The quarks and antiquarks of the constituents of the mesons are produced inside the flux tube, the wave functions need to obey the boundary condition appropriate for the tube. They acquire a transverse momentum distribution governed by the geometry of the tube with a standard deviation  $\sigma_u$  related to the radius of the tube  $R_{\text{tube}}$  by

$$\sigma_u \sim \frac{\hbar}{R_{\text{tube}}}. \quad (15)$$

In addition, the quark and antiquark pair are produced in a Schwinger pair-production mechanism, from which

they acquire a transverse momentum distribution with a standard deviation  $\sigma_q$  given by [13, 14, 18, 20]

$$\sigma_q = \sqrt{\frac{\kappa}{\pi}}, \quad (16)$$

where  $\kappa$  is the strength of the linear color-electric field between the polarizing leading quark and antiquark. By folding of the transverse momentum distribution from the flux tube and the transverse momentum distribution from the Schwinger mechanism, the transverse momentum distribution  $dN_{T_i}$  of each constituent  $\mathbf{p}_{T_i}$  can be given by a Gaussian distribution as

$$\begin{aligned} \frac{dN_{T_i}}{d\mathbf{p}_{T_i}} &= \frac{1}{(\sqrt{2\pi}\sigma_u)^2} \int \frac{d\mathbf{q}}{(\sqrt{2\pi}\sigma_q)^2} \exp\left\{-\frac{\mathbf{q}^2}{2\sigma_q^2}\right\} \exp\left\{-\frac{(\mathbf{p}_{T_i} - \mathbf{q})^2}{2\sigma_u^2}\right\} \\ &= \frac{1}{(\sqrt{2\pi}\sigma)^2} \exp\left\{-\frac{\mathbf{p}_{T_i}^2}{2\sigma^2}\right\}, \end{aligned} \quad (17)$$

where

$$\sigma^2 = \sigma_u^2 + \sigma_q^2. \quad (18)$$

Therefore, when the four constituents  $p_1, p_2, p_3, p_4$  are produced independently without correlations for two non-adjacent mesons, the transverse momentum distribution  $dN_T^N$  of these particles is

$$dN_T^N = \frac{d\mathbf{p}_{T_1} d\mathbf{p}_{T_2} d\mathbf{p}_{T_3} d\mathbf{p}_{T_4}}{(\sqrt{2\pi}\sigma)^8} \exp\left\{-\frac{\mathbf{p}_{T_1}^2 + \mathbf{p}_{T_2}^2 + \mathbf{p}_{T_3}^2 + \mathbf{p}_{T_4}^2}{2\sigma^2}\right\}. \quad (19)$$

For the most likely case in the production of mesons with light quarks with  $m_1=m_2=m_3=m_4$ , the transformations (3) and (12) from  $(\mathbf{p}_{T_i}, \mathbf{p}_{T_j})$  to  $(\mathbf{P}_{T_{ij}}, \mathbf{p}_{T_{ij}})$  can be easily carried out. In terms of the composite transverse momenta and their relative momenta, the momentum distribution (19) becomes

$$\begin{aligned} dN_T^N &= \frac{1}{(\sqrt{2\pi}\sigma)^8} d\mathbf{P}_{T_{12}} d\mathbf{P}_{T_{34}} d\mathbf{p}_{T_{12}} d\mathbf{p}_{T_{34}} \\ &\times \exp\left\{-\frac{1}{2\sigma^2} \left(\frac{\mathbf{P}_{T_{12}}^2}{2} + 2\mathbf{p}_{T_{12}}^2 + \frac{\mathbf{P}_{T_{34}}^2}{2} + 2\mathbf{p}_{T_{34}}^2\right)\right\}. \end{aligned} \quad (20)$$

The relative transverse momenta  $\mathbf{p}_{T_{12}}$  and  $\mathbf{p}_{T_{34}}$  can be integrated out to yield

$$dN_T^N = \frac{d\mathbf{P}_{T_{12}} d\mathbf{P}_{T_{34}}}{4(\sqrt{2\pi}\sigma)^4} \exp\left\{-\frac{1}{2\sigma^2} \left(\frac{\mathbf{P}_{T_{12}}^2}{2} + \frac{\mathbf{P}_{T_{34}}^2}{2}\right)\right\} \quad (21)$$

We represent  $\mathbf{P}_{T_{ij}}$  by  $(p_{T_{ij}}, \phi_{ij})$  and introduce the azimuthal angle difference  $\Delta\phi$  and sum  $\Sigma$ ,

$$\Delta\phi = \phi_{12} - \phi_{34}, \quad \Sigma = \phi_{12} + \phi_{34}. \quad (22)$$

Upon averaging over  $\Sigma$ , we have

$$\begin{aligned} dN_T^N &= \frac{1}{4(\sqrt{2\pi}\sigma)^4} \frac{1}{2} d\Delta\phi \frac{1}{\Sigma_{\max} - \Sigma_{\min}} \int_{\Sigma_{\min}}^{\Sigma_{\max}} d\Sigma \\ &\times \int d\mathbf{P}_{T_{12}} d\mathbf{P}_{T_{34}} \exp\left\{-\frac{1}{2\sigma^2} \left(\frac{\mathbf{P}_{T_{12}}^2}{2} + \frac{\mathbf{P}_{T_{34}}^2}{2}\right)\right\}, \end{aligned}$$

which gives

$$\frac{dN_T^N}{d\Delta\phi} = \frac{1}{8\pi^2}. \quad (23)$$

Consequently, for non-adjacent mesons in the absence of any correlation between the produced quarks and antiquarks, the transverse momentum distribution  $dN_T^N$  is independent of the azimuthal angle difference  $\Delta\phi$  of two non-adjacent mesons.

#### IV. THE TWO-PARTICLE TRANSVERSE DISTRIBUTION FOR ADJACENT MESONS

For two adjacent mesons as shown in Fig. 2, the transverse distribution  $dN_T^N$  in Eq. (19) in the last section will need to be modified to become

$$\begin{aligned} dN_T^A &= dN_q dN_{q'} dN_{q''} \frac{1}{(\sqrt{2\pi}\sigma_u)^8} d\mathbf{p}_{T_1} d\mathbf{p}_{T_2} d\mathbf{p}_{T_3} d\mathbf{p}_{T_4} \\ &\times \exp\left\{-\frac{(\mathbf{p}_{T_1} - \mathbf{q}')^2 + (\mathbf{p}_{T_2} - \mathbf{q})^2 + (\mathbf{p}_{T_3} + \mathbf{q})^2 + (\mathbf{p}_{T_4} - \mathbf{q}'')^2}{2\sigma_u^2}\right\}, \end{aligned} \quad (24)$$

where the momentum kicks  $\mathbf{q}$ ,  $\mathbf{q}'$ , and  $\mathbf{q}''$  of the Schwinger mechanism have the distributions

$$dN_{q_i} = \frac{1}{(\sqrt{2\pi}\sigma_q)^2} d\mathbf{q}_i \exp\left\{-\frac{\mathbf{q}_i^2}{2\sigma_q^2}\right\}, \quad \mathbf{q}_i = \mathbf{q}, \mathbf{q}', \text{ and } \mathbf{q}'' \quad (25)$$

The quark  $p_2$  and the antiquark  $p_3$  in Fig. 2 are produced by the Schwinger mechanism at the point  $V$ . Because of the local conservation of momentum at the production point  $V$ , the transverse momentum  $\mathbf{p}_{T_2}$  and  $\mathbf{p}_{T_3}$  are correlated and the correlation is expressed in Eq. (24) as a shift of their momenta  $\mathbf{p}_{T_2}$  and  $\mathbf{p}_{T_3}$  in Eq. (19) to  $\mathbf{p}_{T_2} - \mathbf{q}$  and  $\mathbf{p}_{T_3} + \mathbf{q}$  respectively. The constituents  $p_1$  and  $p_4$  themselves are products of Schwinger pair production and their transverse momenta  $\mathbf{p}_{T_1}$  and  $\mathbf{p}_{T_4}$  become  $\mathbf{p}_{T_1} - \mathbf{q}'$ , and  $\mathbf{p}_{T_4} - \mathbf{q}''$ , depending on the momentum kicks  $\mathbf{q}'$  and  $\mathbf{q}''$ .

After integrating over  $\mathbf{q}'$  and  $\mathbf{q}''$  in the distributions  $dN_{q'}$  and  $dN_{q''}$  as in Eq. (17), the momentum distribution  $dN_T^A$  in Eq. (24) becomes

$$dN_T^A = dN_q d\tilde{N}_T(q), \quad (26a)$$

$$\begin{aligned} d\tilde{N}_T(q) &= \frac{1}{(\sqrt{2\pi}\sigma)^4} \frac{1}{(\sqrt{2\pi}\sigma_u)^4} d\mathbf{p}_{T_1} d\mathbf{p}_{T_2} d\mathbf{p}_{T_3} d\mathbf{p}_{T_4} \\ &\times \exp\left\{-\frac{\mathbf{p}_{T_1}^2}{2\sigma^2} + \frac{(\mathbf{p}_{T_2} - \mathbf{q})^2 + (\mathbf{p}_{T_3} + \mathbf{q})^2 + \mathbf{p}_{T_4}^2}{2\sigma_u^2}\right\}. \end{aligned} \quad (26b)$$

Our task is to separate out the relevant degrees of freedom in Eq. (26b). The most likely case is the production of mesons with light quarks, for which we can take  $m_1=m_2=m_3=m_4$ . By using the momentum transformations of Eqs. (3) and (12), we convert  $\mathbf{p}_{T_1}$ ,  $\mathbf{p}_{T_2}$ ,  $\mathbf{p}_{T_3}$ , and  $\mathbf{p}_{T_4}$ , to  $\mathbf{p}_{T_{12}}$ ,  $\mathbf{p}_{T_{34}}$ ,  $\mathbf{P}_{T_{12}}$ , and  $\mathbf{P}_{T_{34}}$ . Eq. (26b) becomes

$$\begin{aligned} d\tilde{N}_T(q) &= \frac{1}{(\sqrt{2\pi}\sigma)^4} \frac{1}{(\sqrt{2\pi}\sigma_u)^4} d\mathbf{P}_{T_{12}} d\mathbf{P}_{T_{34}} d\mathbf{p}_{T_{12}} d\mathbf{p}_{T_{34}} \\ &\times \exp\{A + B + C + D + E\}. \end{aligned} \quad (27)$$

where we collect the quadratic function of  $\mathbf{p}_{T12}$  in  $A$ ,

$$A = -\mathbf{p}_{12}^2 \left[ \frac{1}{2\sigma^2} + \frac{1}{2\sigma_u^2} \right] - \mathbf{p}_{12} \cdot \left[ \frac{\mathbf{P}_{12}}{2\sigma^2} + \frac{-\mathbf{P}_{12} + 2\mathbf{q}}{2\sigma_u^2} \right], \quad (28)$$

we collect the quadratic function of  $\mathbf{p}_{T34}$  in  $B$ ,

$$B = -\mathbf{p}_{34}^2 \left[ \frac{1}{2\sigma^2} + \frac{1}{2\sigma_u^2} \right] - \mathbf{p}_{34} \cdot \left[ \frac{-\mathbf{P}_{34}}{2\sigma^2} + \frac{+\mathbf{P}_{34} + 2\mathbf{q}}{2\sigma_u^2} \right], \quad (29)$$

we collect the remaining quadratic function of  $\mathbf{P}_{T12}$  in  $C$ ,

$$C = -\mathbf{P}_{12}^2 \frac{1}{4} \cdot \left[ \frac{1}{2\sigma^2} + \frac{1}{2\sigma_u^2} \right] - \mathbf{P}_{12} \cdot \left[ \frac{-\mathbf{q}}{2\sigma_u^2} \right], \quad (30)$$

we collect the remaining quadratic function of  $\mathbf{P}_{T34}$  in  $D$ ,

$$D = -\mathbf{P}_{34}^2 \frac{1}{4} \cdot \left[ \frac{1}{2\sigma^2} + \frac{1}{2\sigma_u^2} \right] - \mathbf{P}_{34} \cdot \left[ \frac{+\mathbf{q}}{2\sigma_u^2} \right] \quad (31)$$

and the last term quadratic in  $\mathbf{q}^2$  in  $E$ ,

$$E = -\frac{2\mathbf{q}^2}{2\sigma_u^2}. \quad (32)$$

By completing the squares of  $A$  and  $B$  in Eqs. (28) and (29), the integration over  $\mathbf{p}_{T12}$  and  $\mathbf{p}_{T34}$  can be carried out analytically, yielding a function of  $\mathbf{P}_{T12}$ ,  $\mathbf{P}_{T34}$ , and  $\mathbf{q}$ . After these integrations, we obtain

$$\begin{aligned} d\tilde{N}(q) &= \frac{1}{(2\pi)^2(\sigma^2 + \sigma_u^2)^2} d\mathbf{P}_{12} d\mathbf{P}_{34} \\ &\times \exp \left\{ \frac{\sigma_{12}^2}{2} \left[ \frac{-\sigma_q^2 \mathbf{P}_{T12} + \mathbf{q}}{2\sigma^2 \sigma_u^2} + \frac{\mathbf{q}}{\sigma_u^2} \right]^2 + \frac{\sigma_{12}^2}{2} \left[ \frac{+\sigma_q^2 \mathbf{P}_{34} + \mathbf{q}}{2\sigma^2 \sigma_u^2} + \frac{\mathbf{q}}{\sigma_u^2} \right]^2 \right\} \\ &\times \exp \left\{ -\frac{\mathbf{P}_{12}^2}{8\sigma_{12}^2} + \frac{\mathbf{P}_{12} \cdot \mathbf{q}}{2\sigma_u^2} - \frac{\mathbf{P}_{34}^2}{8\sigma_{12}^2} - \frac{\mathbf{P}_{34} \cdot \mathbf{q}}{2\sigma_u^2} - \frac{\mathbf{q}^2}{\sigma_u^2} \right\}. \quad (33) \end{aligned}$$

For the remaining degrees of freedom, we define  $\phi_{12}$  as the azimuthal angle between  $\mathbf{q}$  and  $\mathbf{P}_{T12}$ , and  $\phi_{34}$  as the azimuthal angle between  $\mathbf{q}$  and  $\mathbf{P}_{T34}$ . We form the sum and the difference of the azimuthal angles

$$\Delta\phi = \phi_{12} - \phi_{34}, \quad \Sigma = \phi_{12} + \phi_{34}, \quad (34a)$$

$$\phi_{12} = \frac{1}{2}(\Sigma + \Delta\phi), \quad \phi_{34} = \frac{1}{2}(\Sigma - \Delta\phi). \quad (34b)$$

We then get the distribution  $d\tilde{N}_T(q)$  defined in the intervals  $-\pi \leq \Delta\phi \leq \pi$  and  $\Sigma_{\min}(\Delta\phi) \leq \Sigma \leq \Sigma_{\max}(\Delta\phi)$  where

$$\Sigma_{\min}(\Delta\phi) = -2\pi + |\Delta\phi|, \quad (35a)$$

$$\Sigma_{\max}(\Delta\phi) = -|\Delta\phi| + 2\pi. \quad (35b)$$

Normalized distribution per pair of mesons  $P_{12}$  and  $P_{34}$  is

$$\begin{aligned} \frac{d\tilde{N}_T(q)}{d\Delta\phi}(\Delta\phi) &= \frac{1}{(\Sigma_{\max} - \Sigma_{\min})} \int_{\Sigma_{\min}}^{\Sigma_{\max}} d\Sigma \frac{P_{T12} dP_{T12} P_{T34} dP_{T34}}{2(2\pi)^2(\sigma^2 + \sigma_u^2)^2} \\ &\times \exp \left\{ \frac{\sigma_{12}^2}{2} \left[ \frac{-\sigma_q^2 \mathbf{P}_{T12} + \mathbf{q}}{2\sigma^2 \sigma_u^2} + \frac{\mathbf{q}}{\sigma_u^2} \right]^2 + \frac{\sigma_{12}^2}{2} \left[ \frac{+\sigma_q^2 \mathbf{P}_{34} + \mathbf{q}}{2\sigma^2 \sigma_u^2} + \frac{\mathbf{q}}{\sigma_u^2} \right]^2 \right\} \\ &\times \exp \left\{ -\frac{\mathbf{P}_{12}^2}{8\sigma_{12}^2} + \frac{\mathbf{P}_{12} \cdot \mathbf{q}}{2\sigma_u^2} - \frac{\mathbf{P}_{34}^2}{8\sigma_{12}^2} - \frac{\mathbf{P}_{34} \cdot \mathbf{q}}{2\sigma_u^2} - \frac{\mathbf{q}^2}{\sigma_u^2} \right\}. \quad (36) \end{aligned}$$

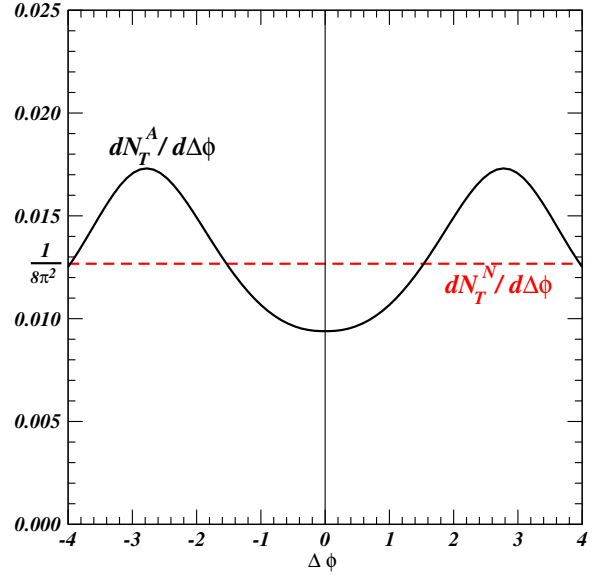


FIG. 4. (Color online) The transverse momentum distributions as a function of the difference  $\Delta\phi$  of the azimuthal angles between two adjacent mesons,  $dN_T^A/d\Delta\phi$ , and two non-adjacent mesons,  $dN_T^N/d\Delta\phi$ .

where the scalar product  $\mathbf{P}_{Tij} \cdot \mathbf{q}$  is

$$\mathbf{P}_{Tij} \cdot \mathbf{q} = P_{Tij} q \cos(\phi_{ij}). \quad (37)$$

Here,  $\phi_{12}$  and  $\phi_{34}$  in the integrand can be expressed as a function of  $\Delta\phi$  and  $\Sigma$  as given by Eq. (34b). We can calculate  $d\tilde{N}_T(q)/d\Delta\phi$  by integrating out  $\Sigma$ ,  $P_{T12}$ , and  $P_{T34}$  in the above equation, and we obtain  $d\tilde{N}_T(q)/d\Delta\phi$  for different values of  $q$ . We need the values of  $\sigma_u$ , and  $\sigma_q$  to get the numerical estimate. For a flux tube radius of  $R_{\text{tube}} = 0.6$  fm and  $\kappa = 1$  GeV/fm, we get  $\sigma_u = 0.33$  GeV/c,  $\sigma_q = 0.25$  GeV/c, and  $\sigma = 0.414$  GeV/c.

One finds that the distribution  $d\tilde{N}_T(q)/d\Delta\phi$  depends on the magnitude of the momentum  $|\mathbf{q}|/\sigma_q$  whose distribution is given by Eq. (25). Upon integrating the distribution of  $q$ , we obtain the distribution of  $\Delta\phi$  for two adjacently produced mesons  $P_{12}$  and  $P_{34}$ ,

$$\frac{dN_T^A}{d\Delta\phi} = \int \frac{dq}{(\sqrt{2\pi}\sigma_q)^2} \exp\left\{-\frac{q^2}{2\sigma_q^2}\right\} \frac{d\tilde{N}_T(q)}{d\Delta\phi}. \quad (38)$$

The solid curve in Fig. 4 is the  $dN_T^A/d\Delta\phi$  result obtained by a direct numerical integration over  $q$ . The correlation is suppressed on the near side at  $\Delta\phi \sim 0$ , and is enhanced on the back-to-back away side at  $\Delta\phi \sim \pi$ . Such a result is expected because the quark  $p_2$  and the antiquark  $p_3$  are produced in opposite azimuthal directions due to the local momentum conservation. The associated adjacently produced mesons  $P_{12}$  and  $P_{34}$  should also have back-to-back azimuthal correlations.

Along with the correlation for an adjacent pair of mesons, there is also the azimuthal angular correlation  $dN_T^N/d\Delta\phi$  for a pair of non-adjacent mesons in a flux tube fragmentation. The angular correlation  $dN_T^N/d\Delta\phi$

corresponds to the case where the quark  $p_2$  and the antiquark  $p_3$  are not correlated by the momentum  $\mathbf{q}$ . It is given by Eq. (23) with  $dN_T^N/d\Delta\phi=1/8\pi^2$ . It can also be alternatively obtained by setting  $q=0$  in Eq. (36).

The above results have been obtained by applying the local law of conservation of momentum for a system of equal quark masses. As the constituent quark mass of a strange quark is only slightly greater than the constituent quark masses of the up and down quarks [53], the qualitative feature of the above results regarding a back-to-back correlation for adjacent meson production may also be applicable to cases involving the production of strange mesons.

## V. RAPIDITY CORRELATION OF PRODUCED MESONS IN A FLUX TUBE FRAGMENTATION

The last section gives the azimuthal correlation of two adjacent and non-adjacent mesons in a flux tube fragmentation. How do we identify adjacent and non-adjacent pairs of mesons? We shall use the space-time-rapidity ordering to correlate the rapidities of produced mesons with the spatial locations on the flux tube at the moment of fragmentation.

Casher *et al.* [5] showed that in QED2 when a quark parton pulls away from an antiquark with the speed of light, the produced dipole density of produced  $q\bar{q}$  pairs is a Lorentz-invariant function and the lines of constant produced dipole density of produced  $q\bar{q}$  pairs are hyperbolas with constant proper times. It is therefore reasonable to assume as a first approximation that the space-time distribution of the  $q\bar{q}$  production vertices should depend only on the vertex production proper time,  $\tau_{pro}$ , relative to the point of the onset of separation of the leading quark and antiquark.

Previously in [16] and in Exercise (7.1) of [20], we show that if all the pair-production vertices of a fragmenting string falls on the curve of the proper time  $\tau_{pro}$ , the rapidity distribution of the produced mesons is a constant given by

$$\frac{dN}{dy} = \frac{\kappa\tau_{pro}}{m_T}, \quad (39)$$

where  $\kappa$  is the string tension and  $m_T$  is the transverse mass of the particle  $m_T = \sqrt{m^2 + p_T^2}$  where  $m$  is the mass of a produced meson (mostly likely a meson). Thus the presence of a rapidity plateau is an indication of the approximate validity of the occurrence of the  $q\bar{q}$  vertices along a curve of constant proper time. We show further in Exercise (7.2) of [20] that in that case, the produced particles are ordered in space-time-rapidity. The ordering of produced particles means that in the center-of-mass system, particles with a greater magnitude of rapidity  $|y|$  are produced at a distance farther away from the point of collision and at a time later than and more separated from the time of collision, as shown in Fig. 5. From such a picture of flux tube fragmentation, we envis-

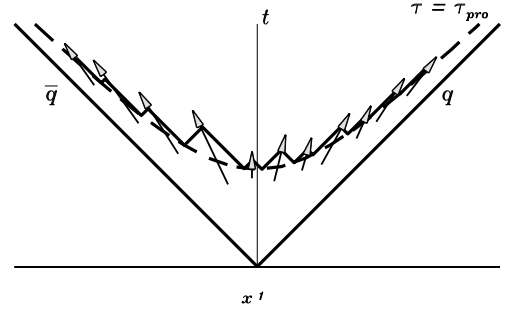


FIG. 5. (Figure taken from Figure 6.4 of [20]). The space-time trajectories of the leading quark  $q$  moving to the positive  $x^1$ -direction (longitudinal direction) and the antiquark moving to the negative  $x^1$  direction, with the production of  $q\bar{q}$  pairs lying on the proper time curve of constant  $\tau_{pro}$ . A produced  $q$  at one vertex interact with the produced  $\bar{q}$  in the adjacent vertex to form a meson. The trajectories of mesons are indicated by thick arrows. The rapidities of the produced mesons are ordered along the spatial longitudinal  $x^1$ -axis, and in time.

age that produced mesons are ordered in space-time and in rapidity, with mesons that are produced adjacent to each other closest in their magnitudes of their rapidity values [20]. Therefore, mesons that are produced adjacent to each other if their rapidity difference  $\Delta y$  fall within a rapidity width  $w$ ,

$$|\Delta y| \lesssim w, \quad (40)$$

where  $w$  is the rapidity per produced meson,

$$w = \frac{1}{dN/dy} \sim \frac{1}{(3/2)dN_{ch}/dy}. \quad (41)$$

One notes from Eq. (39) that the width  $w$  is inversely proportional to the particle production time  $\tau_{pro}$ . As the particle production time cannot be sharp and has a distribution (see Fig. 2 of [16] for an example of the scatter plot of the pair production vertex proper times in the Lund Model), the width  $w$  would also have a distribution. The condition relating  $\Delta y$  with adjacently produced mesons should also have a diffuseness described by an additional parameter  $a$ . Therefore, within the nearest-neighbor rapidity width  $|\Delta y| \lesssim w$  in the central rapidity region, the produced mesons are adjacent to each other and the rapidity correlation for an adjacent pair of mesons is

$$\frac{dN_y^A}{d\Delta y} = \frac{1}{1 + e^{(|\Delta y| - w)/a}}. \quad (42)$$

Upon approximating the rapidity  $y$  as the pseudorapidity  $\eta$ , the above correlation for adjacent pair becomes

$$\frac{dN_\eta^A}{d\Delta\eta} = \frac{1}{1 + e^{(|\Delta\eta| - w)/a}}. \quad (43)$$



The complete correlation consists of both the transverse and longitudinal correlations. From the transverse azimuthal correlation  $dN_T^A/d\Delta\phi$  for adjacent mesons as given in Fig. 4, we have therefore the two-particle angular correlation for an adjacent pair of mesons as

$$\frac{dN^A}{d\Delta\phi d\Delta\eta} = \frac{dN_T^A}{d\Delta\phi} \frac{dN_\eta^A}{d\Delta\eta} = \frac{1}{1 + e^{(|\Delta\eta|-w)/a}} \frac{dN_T^A}{d\Delta\phi}. \quad (44)$$

On the other hand, outside this nearest-neighbor rapidity width with  $|\Delta\eta| \lesssim w$ , the two mesons are non-adjacent. The condition of being a non-adjacent pair, outside the nearest-neighbor rapidity width with  $|\Delta\eta| \lesssim w$  can be specified by  $1/(1 + e^{(w-|\Delta\eta|)/a})$ . Consequently, the two-particle pseudorapidity correlation for a non-adjacent pair of mesons in a flux tube fragmentation is

$$\frac{dN_\eta^N}{d\Delta\eta} = \frac{1}{1 + e^{(w-|\Delta\eta|)/a}}. \quad (45)$$

From the transverse azimuthal correlation  $dN_T^N/d\Delta\phi$  as given in Eq. (23), we have therefore the two-particle angular correlation for a non-adjacent pair of mesons as

$$\frac{dN^N}{d\Delta\phi d\Delta\eta} = \frac{dN_T^N}{d\Delta\phi} \frac{dN_\eta^N}{d\Delta\eta} = \frac{1}{1 + e^{(w-|\Delta\eta|)/a}} \frac{1}{8\pi^2}. \quad (46)$$

In experimental measurements, one selects a pair of mesons whose charges and heavy quark quantum numbers can be the same or opposite. Different selections will result in different adjacent and non-adjacent fractions, and consequently different linear combinations of  $dN^A/d\Delta\phi d\Delta\eta$  and  $dN^N/d\Delta\phi d\Delta\eta$ . They will lead to different shapes of the correlation functions. It is necessary to find out the adjacent and non-adjacent fractions for different charge and heavy quark configurations.

## VI. CHARGE CORRELATION IN FLUX TUBE FRAGMENTATION FOR QUARKS WITH TWO FLAVORS

In a flux tube fragmentation, the production of the quark-antiquark pair  $p_2$  and  $p_3$  at the local point  $V$  in Fig. 2 must satisfy local charge and flavor conservations. This means that  $p_2$  and  $p_3$  must be quark and antiquark with opposite charges and flavor quantum numbers. Such a local conservation will induce correlations on charges and flavors of adjacent mesons. For non-adjacent mesons, there will be no such correlations.

We can investigate all possible charge and flavor contents of two produced mesons if they are in the adjacent or non-adjacent state. We study the case of quarks with two flavors in this section, and the case with three flavors in the next section.

We examine first the production of two adjacent mesons and construct in Table I all possible meson production configurations in which the quark  $p_2$  and the antiquark  $p_3$  have different combinations of charges and

flavor quantum numbers. Here,  $Q_{ij}$  is the charge of the composite meson  $P_{ij}$  with constituents  $p_i$  and  $p_j$ .

There are altogether eight possible cases in Table I. The number of cases  $N^A(Q_{12}, Q_{34})$  and the associated probabilities  $P^A(Q_{12}, Q_{34})$  in different charge configurations  $(Q_{12}, Q_{34})$  for two adjacent mesons in a flux tube fragmentation are given in Table II. We note that because  $p_2$  and  $p_3$  have equal and opposite charges, two adjacently produced mesons  $P_{12}$  and  $P_{34}$  cannot have charges of the same sign as shown in Table II.

TABLE I. Quark and antiquark configurations for two adjacently produced mesons in a flux tube fragmentation where  $p_2$  and  $p_3$  are constrained by local charge conservation and flavor balance.

$p_1$	$p_2$	$Q_{12}$	$p_3$	$p_4$	$Q_{34}$
$\bar{u}$	$u$	0	$\bar{u}$	$d$	-1
$\bar{d}$	$u$	1	$\bar{u}$	$d$	-1
$\bar{u}$	$u$	0	$\bar{u}$	$u$	0
$\bar{d}$	$u$	1	$\bar{u}$	$u$	0
$\bar{u}$	$d$	-1	$\bar{d}$	$d$	0
$\bar{d}$	$d$	0	$\bar{d}$	$d$	0
$\bar{u}$	$d$	-1	$\bar{d}$	$u$	1
$\bar{d}$	$d$	0	$\bar{d}$	$u$	1

TABLE II. The number of cases  $N^A(Q_{12}, Q_{34})$  and the probability  $P^A(Q_{12}, Q_{34})$  of the charge configurations for two adjacently produced mesons in a flux tube fragmentation.

		$Q_{34}=-1$	$Q_{34}=0$	$Q_{34}=1$
$N^A(Q_{12}, Q_{34})$	$Q_{12}=-1$	0	1	1
	$Q_{12}=0$	1	2	1
	$Q_{12}=+1$	1	1	0
$P^A(Q_{12}, Q_{34})$	$Q_{12}=-1$	0	0.125	0.125
	$Q_{12}=0$	0.125	0.250	0.125
	$Q_{12}=+1$	0.125	0.125	0

We next examine the production of two mesons in the non-adjacent state. We construct in Table III all charge configurations of two non-adjacent mesons. In that case, the charge and flavor quantum numbers of quark  $p_2$  and antiquark  $p_3$  need not be correlated. Without the constraint on the flavors of  $p_2$  and  $p_3$ , one has altogether 16 possible cases as listed in Table III. The number of cases  $N^N(Q_{12}, Q_{34})$  and the associated probabilities  $P^N(Q_{12}, Q_{34})$  in different charge configurations  $(Q_{12}, Q_{34})$  for two non-adjacent mesons in a flux tube fragmentation are given in Table IV. In this case, there is an equal probability for two non-adjacent mesons  $P_{12}$  and  $P_{34}$  to have charges of the same sign or opposite signs. This is in contrast to adjacent mesons for which there is no probability of their charges to be of the same sign.

TABLE III. Quark and antiquark configurations for two non-adjacent mesons in flux tube fragmentation where  $p_2$  and  $p_3$  are not constrained by flavor balance and local charge conservation.

$p_1$	$p_2$	$Q_{12}$	$p_3$	$p_4$	$Q_{34}$
$\bar{u}$	$u$	0	$\bar{u}$	$d$	-1
$\bar{d}$	$u$	1	$\bar{u}$	$d$	-1
$\bar{u}$	$u$	0	$\bar{u}$	$u$	0
$\bar{d}$	$u$	1	$\bar{u}$	$u$	0
$\bar{u}$	$d$	-1	$\bar{d}$	$d$	0
$\bar{d}$	$d$	0	$\bar{d}$	$d$	0
$\bar{u}$	$d$	-1	$\bar{d}$	$u$	1
$\bar{d}$	$d$	0	$\bar{d}$	$u$	1
$\bar{u}$	$u$	0	$\bar{d}$	$d$	0
$\bar{d}$	$u$	1	$\bar{d}$	$d$	0
$\bar{u}$	$u$	0	$\bar{d}$	$u$	1
$\bar{d}$	$u$	1	$\bar{d}$	$u$	1
$\bar{u}$	$d$	-1	$\bar{u}$	$d$	-1
$\bar{d}$	$d$	0	$\bar{u}$	$d$	-1
$\bar{u}$	$d$	-1	$\bar{u}$	$u$	0
$\bar{d}$	$d$	0	$\bar{u}$	$u$	0

TABLE IV. The number of cases  $N^N(Q_{12}, Q_{34})$  and the probability  $P^N(Q_{12}, Q_{34})$  of all charge configurations for two non-adjacent mesons  $P_{12}$  and  $P_{34}$  in a flux tube fragmentation.

		$Q_{34}=-1$	$Q_{34}=0$	$Q_{34}=1$
$N^N(Q_{12}, Q_{34})$	$Q_{12}=-1$	1	2	1
	$Q_{12}=0$	2	4	2
	$Q_{12}=+1$	1	2	1
$P^N(Q_{12}, Q_{34})$	$Q_{12}=-1$	0.0625	0.125	0.0625
	$Q_{12}=0$	0.125	0.250	0.125
	$Q_{12}=+1$	0.0625	0.125	0.0625

The charge pattern for two produced mesons in the adjacent state is quite different from the charge pattern of mesons in the non-adjacent state, in a flux tube fragmentation.

## VII. CHARGE AND FLAVOR CORRELATION IN FLUX TUBE FRAGMENTATION FOR QUARKS WITH WITH THREE FLAVORS

The considerations in the last section for the production of  $u\bar{u}$  and  $d\bar{d}$  pairs can be generalized to the case with the additional production of  $s\bar{s}$  pairs. Compared to the production of a  $u$  or  $d$  quark pair, the probability for the production of a strange quark pair is suppressed by a strangeness suppression factor  $f_s$  that is energy dependent [46–49, 64–67], and is of order 0.10 at  $\sqrt{s_{NN}}=200$  GeV as shown in Appendix A. We can enumerate all charge configurations in a flux tube fragmentation, for both adjacent and non-adjacent mesons. The additional strangeness degree of freedom brings in an additional correlation of the strange quantum numbers of the produced mesons.

In enumerating all possible configurations for the production of two mesons, it is useful to associate each configuration by the order of the strangeness suppression factor  $f_s$ . Basing the probability for light  $q\bar{q}$  production to be a unit with unit order 1 and referring to the constituents in Fig. 2 for adjacent mesons and Fig. 3 for non-adjacent mesons, the production of an  $\bar{s}$  in  $p_1$  or an  $s$  quark in  $p_4$  will each bring in a suppression factor of order  $f_s$ . Similarly, the production of an  $s$  in  $p_2$  and an  $\bar{s}$  in  $p_3$  in two non-adjacent mesons will also each bring in a factor of  $f_s$ . However, the production of an  $s$  in  $p_2$  and an  $\bar{s}$  in  $p_3$  in adjacent mesons will bring in altogether only a single factor of  $f_s$  because this  $s\bar{s}$  pair arise from a single Schwinger pair production mechanism. From these considerations, we can construct all possible mesons charges ( $Q_{12}, Q_{34}$ ) and meson strangeness ( $S_{12}, S_{34}$ ) up to first order in  $f_s$  in Table V for adjacent meson pairs. Here,  $S_{ij}$  is the strangeness of the composite meson  $P_{ij}$  with constituents  $p_i$  and  $p_j$ .

TABLE V. Quark, antiquark, charge, and strangeness configurations for two adjacent mesons in a flux tube fragmentation, where  $p_2$  and  $p_3$  are constrained by charge and flavor balance, for flux tube fragmentation with three flavors.

$p_1$	$p_2$	$Q_{12}$	$S_{12}$	$p_3$	$p_4$	$Q_{34}$	$S_{34}$	order
$\bar{u}$	$u$	0	0	$\bar{u}$	$d$	-1	0	1
$\bar{d}$	$u$	1	0	$\bar{u}$	$d$	-1	0	1
$\bar{u}$	$u$	0	0	$\bar{u}$	$u$	0	0	1
$\bar{d}$	$u$	1	0	$\bar{u}$	$u$	0	0	1
$\bar{u}$	$d$	-1	0	$\bar{d}$	$d$	0	0	1
$\bar{d}$	$d$	0	0	$\bar{d}$	$d$	0	0	1
$\bar{u}$	$d$	-1	0	$\bar{d}$	$u$	1	0	1
$\bar{d}$	$d$	0	0	$\bar{d}$	$u$	1	0	1
$\bar{u}$	$s$	-1	-1	$\bar{s}$	$d$	0	1	$f_s$
$\bar{d}$	$s$	0	-1	$\bar{s}$	$d$	0	1	$f_s$
$\bar{u}$	$s$	-1	-1	$\bar{s}$	$u$	1	1	$f_s$
$\bar{d}$	$s$	0	-1	$\bar{s}$	$u$	1	1	$f_s$
$\bar{s}$	$u$	1	1	$\bar{u}$	$d$	-1	0	$f_s$
$\bar{s}$	$u$	1	1	$\bar{u}$	$u$	0	0	$f_s$
$\bar{u}$	$u$	0	0	$\bar{u}$	$s$	-1	-1	$f_s$
$\bar{d}$	$u$	1	0	$\bar{u}$	$s$	-1	-1	$f_s$
$\bar{s}$	$d$	0	1	$\bar{d}$	$d$	0	0	$f_s$
$\bar{s}$	$d$	0	1	$\bar{d}$	$u$	1	0	$f_s$
$\bar{u}$	$d$	-1	0	$\bar{d}$	$s$	0	-1	$f_s$
$\bar{d}$	$d$	0	0	$\bar{d}$	$s$	0	-1	$f_s$

From the above Table V, we can construct the number of different charge configurations in Table VI for two adjacent mesons in in a flux tube fragmentation with three flavors. Here, the superscript ( $ud$ ) specifies the  $ud$  sector, and ( $s$ ) the strange sector.

TABLE VI. Up to order  $f_s$ , the number of cases  $N^{A(ud)}(Q_{12}, Q_{34})$  and  $N^{A(s)}(Q_{12}, Q_{34})$  for different charge configurations  $(Q_{12}, Q_{34})$ , in two adjacent mesons  $P_{12}$  and  $P_{34}$  in a flux tube fragmentation with three flavors.

		$Q_{34}=-1$	$Q_{34}=0$	$Q_{34}=1$
$N^{A(ud)}(Q_{12}, Q_{34})$	$Q_{12}=-1$	0	1	1
	$Q_{12}=0$	1	2	1
	$Q_{12}=1$	1	1	0
$N^{A(s)}(Q_{12}, Q_{34})$	$Q_{12}=-1$	0	$2f_s$	$f_s$
	$Q_{12}=0$	$f_s$	$3f_s$	$2f_s$
	$Q_{12}=1$	$2f_s$	$f_s$	0

In a flux tube fragmentation, there is a local conservation of strangeness or heavy quark flavor in the production of a  $Q\bar{Q}$  pair in the flux tube, similar to the conservation of charge. Hence, there are also correlations that arise from strangeness and heavy quark conservation in a flux tube fragmentation. We present in Table VII the number of cases for the production of strangeness configurations  $(S_{12}, S_{34})$ , in a flux tube fragmentation with three flavors.

TABLE VII. The number of cases  $N^{A(ud)}(S_{12}, S_{34})$  and  $N^{A(s)}(S_{12}, S_{34})$  for different strangeness configurations  $(S_{12}, S_{34})$ , for two adjacent mesons  $P_{12}$  and  $P_{34}$  in a flux tube fragmentation with three flavors.

		$S_{34}=-1$	$S_{34}=0$	$S_{34}=1$
$N^{A(s)}(S_{12}, S_{34})$	$S_{12}=-1$	0	0	$4f_s$
	$S_{12}=0$	$4f_s$	0	0
	$S_{12}=1$	0	$4f_s$	0

From the above Table VI, the probability  $P^{A(ud,s)}(Q_{12}, Q_{34})$  for the occurrence of adjacent non-strange mesons ( $ud$ ) and strange mesons ( $s$ ), with charges  $(Q_{12}, Q_{34})$  is related to the number of cases  $N^{A(ud,s)}(Q_{12}, Q_{34})$  in flux tube fragmentation with three flavors by

$$P^{A(ud,s)}(Q_{12}, Q_{34}) = \frac{N^{A(ud,s)}(Q_{12}, Q_{34})}{8 + 12f_s}, \quad (47)$$

which is normalized to

$$\sum_{Q_{12}, Q_{34}} [P^{A(ud)}(Q_{12}, Q_{34}) + P^{A(s)}(Q_{12}, Q_{34})] = 1. \quad (48)$$

Similarly, if one considers the strangeness configurations of two adjacent mesons, the probability  $P^{A(ud,s)}(S_{12}, S_{34})$  for the occurrence of strange mesons with strangeness  $(S_{12}, S_{34})$  is related to the number of cases  $N^{A(ud,s)}(S_{12}, S_{34})$  in flux tube fragmentation with three flavors by

$$P^{A(s)}(S_{12}, S_{34}) = \frac{N^{A(s)}(S_{12}, S_{34})}{8 + 12f_s}. \quad (49)$$

In a similar manner, we can investigate all possible quark, antiquark, charge, and strangeness configurations for two non-adjacent mesons  $P_{12}$  and  $P_{34}$  in a

flux tube fragmentation. In that case, the charge and flavor of  $p_3$  will not need to be correlated with those of  $p_2$ . The details of the enumeration is presented in Appendix B. Again, we need to keep track of the order of the strangeness suppression factor  $f_s$  in different configurations. Keeping configurations only up to the first order in  $f_s$ , we list as a summary the number of cases  $N^{N(ud)}$  and  $N^{N(s)}$  for different combinations of charge and strangeness configurations in Tables VIII and IX respectively.

TABLE VIII. Up to order  $f_s$ , the number of cases  $N^{N(ud)}(Q_{12}, Q_{34})$  and  $N^{N(s)}(Q_{12}, Q_{34})$  of the charge configurations for two non-adjacent mesons  $P_{12}$  and  $P_{34}$  in a flux tube fragmentation with three flavors.

		$Q_{34}=-1$	$Q_{34}=0$	$Q_{34}=1$
$N^{N(ud)}(Q_{12}, Q_{34})$	$Q_{12}=-1$	1	2	1
	$Q_{12}=0$	2	4	2
	$Q_{12}=1$	1	2	1
$N^{N(s)}(Q_{12}, Q_{34})$	$Q_{12}=-1$	$2f_s$	$4f_s$	$2f_s$
	$Q_{12}=0$	$4f_s$	$8f_s$	$4f_s$
	$Q_{12}=1$	$2f_s$	$4f_s$	$2f_s$

We present in Table IX the number of cases for the production of strangeness configurations  $(S_{12}, S_{34})$  for two non-adjacent mesons in a flux tube fragmentation with three flavors.

TABLE IX. The number of cases  $N^{N(ud)}(S_{12}, S_{34})$  and  $N^{N(s)}(S_{12}, S_{34})$  of the strangeness configurations of two non-adjacent mesons in a flux tube fragmentation with three flavors.

		$S_{34}=-1$	$S_{34}=0$	$S_{34}=1$
$N^{N(s)}(S_{12}, S_{34})$	$S_{12}=-1$	0	$8f_s$	0
	$S_{12}=0$	$8f_s$	0	$8f_s$
	$S_{12}=1$	0	$8f_s$	0

From the above Table VIII, we can sum up all possible number of cases, and get the probability  $P^{N(ud,s)}(Q_{12}, Q_{34})$  for non-adjacent mesons. The probabilities for the occurrence of non-strange mesons ( $ud$ ) and strange mesons ( $s$ ), with charges  $(Q_{12}, Q_{34})$  for flux tube fragmentation with three flavors is related to the number of cases  $N^{N(ud,s)}(Q_{12}, Q_{34})$  by

$$P^{N(ud,s)}(Q_{12}, Q_{34}) = \frac{N^{N(ud,s)}(Q_{12}, Q_{34})}{16 + 32f_s}, \quad (50)$$

which is normalized to

$$\sum_{Q_{12}, Q_{34}} [P^{N(ud)}(Q_{12}, Q_{34}) + P^{N(s)}(Q_{12}, Q_{34})] = 1. \quad (51)$$

We also have the probability  $P^{N(ud,s)}(S_{12}, S_{34})$  for non-adjacent mesons with strangeness  $(S_{12}, S_{34})$  for flux tube fragmentation with three flavors given by

$$P^{N(ud,s)}(S_{12}, S_{34}) = \frac{N^{N(ud,s)}(S_{12}, S_{34})}{16 + 32f_s}. \quad (52)$$

### VIII. TWO-MESON CORRELATION FUNCTION IN DIFFERENT CHARGE AND STRANGENESS CONFIGURATIONS

The results in the last few sections allow us to provide different signatures for a color flux tube fragmentation. One measures the  $\Delta\phi$ - $\Delta\eta$  correlations for a given charge or strangeness configuration  $\nu$  within a  $p_T$  domain of interest, the pattern of the correlation will reveal the nature of the reaction mechanism within that  $p_T$  domain, as in the case for the hard-scattering process for  $p_T > 0.5$  GeV/c in Fig. 1.

To specify a charge or strangeness configuration  $\nu$ , one can choose a pair of mesons with electric charges of the same sign, for which  $Q_{12}=Q_{34}$ , of opposite sign, for which  $Q_{12}=-Q_{34}$ , with the same strangeness, for which  $S_{12}=S_{34}$ , with opposite strangeness, for which  $S_{12}=-S_{34}$ , or the correlation of a strange meson with a non-strange meson. Different choices will yield different probabilities  $P^A$  and  $P^N$  for finding adjacent or non-adjacent pair of mesons, and will lead to different patterns of the correlation function, in the fragmentation of a color flux tube.

We can write down the two-meson distribution function  $dN/d\Delta\phi d\Delta\eta$  for a pair of mesons with azimuthal angle difference  $\Delta\phi$  and pseudorapidity difference  $\Delta\eta$  in a charge configuration (or strangeness configuration)  $\nu$  within a given  $p_T$  domain in flux tube fragmentation as given by

$$\frac{dN(\nu)}{d\Delta\phi d\Delta\eta} = \frac{dN^A}{d\Delta\phi d\Delta\eta} \times P^A(\nu) + \frac{dN^N}{d\Delta\phi d\Delta\eta} \times P^N(\nu). \quad (53)$$

Here, the first factor in each term,  $dN^X/d\Delta\phi d\Delta\eta$ , is the distribution function as a function of  $\Delta\phi$  and  $\Delta\eta$ , when the meson pair is an adjacent pair with  $X=A$  or a non-adjacent pair with  $X=N$ , in the fragmentation of the flux tube, as given by Eqs. (44) and (46). The second factor  $P^X(\nu)$  in each term specifies the probability for the pair of mesons in the  $X$  state to be in the configuration  $\nu$  of interest. The total probability  $P^X(\nu)$  for the charge configuration  $\nu$  in meson pairs in the state  $X$  is given by

$$P^X(\nu) = \sum_{(Q_{12}, Q_{34}) \in \nu} [P^{X(ud)}(Q_{12}, Q_{34}) + P^{X(s)}(Q_{12}, Q_{34})]. \quad (54)$$

The total probability  $P^X(\nu)$  for the strangeness configuration  $\nu$  to be in the state  $X$  is given by

$$P^X(\nu) = \sum_{(S_{12}, S_{34}) \in \nu} [P^{X(ud)}(S_{12}, S_{34}) + P^{X(s)}(S_{12}, S_{34})]. \quad (55)$$

The quantities  $P^{X(ud,s)}(S_{12}, S_{34})$  and  $P^{X(ud,s)}(Q_{12}, Q_{34})$  are given by Eqs. (47)-(52) and Tables VI-IX.

We can consider the configuration  $\nu$  of two mesons with charges of opposite signs. We obtain from Table VI for

adjacent mesons and Eq. (47),

$$P^A(\text{opposite charge}) = \frac{2 + 3f_s}{8 + 12f_s} = \frac{1}{4}, \quad (56)$$

and from Table VIII for non-adjacent mesons and Eq. (50),

$$P^N(\text{opposite charge}) = \frac{2 + 4f_s}{16 + 32f_s} = \frac{1}{8}. \quad (57)$$

Similarly, for the charge configuration  $\nu$  of two mesons with charges of the same sign, we obtain from Table VI for adjacent mesons and Eq. (47)

$$P^A(\text{same charge}) = 0, \quad (58)$$

and from Table VIII for non-adjacent mesons and Eq. (50),

$$P^N(\text{same charge}) = \frac{2 + 4f_s}{16 + 32f_s} = \frac{1}{8}. \quad (59)$$

These probabilities for different charge configurations are independent of  $f_s$ , indicating that they can be obtained by considering either two flavors or three flavors. On the other hand, the probability for different strangeness configurations must be obtained by considering three flavors.

We list below the probabilities ( $P^A(\nu), P^N(\nu)$ ) for a few two-meson configurations  $\nu$ :

1.  $\nu$ =(two mesons with charges of opposite signs),  
 $(P^A, P^N)(\text{opposite charge}) = (0.25, 0.125). \quad (60)$

2.  $\nu$ =(two mesons with charges of the same sign),  
 $(P^A, P^N)(\text{same charge}) = (0, 0.125). \quad (61)$

3.  $\nu$ =(two charged mesons ( $Q_{12} \neq 0$  and  $Q_{34} \neq 0$ )),  
 $(P^A, P^N)(\text{all charge}) = (0.25, 0.25), \quad (62)$

which is the sum of the first two cases.

4.  $\nu$ =(two mesons with opposite strangeness),  
 $(P^A, P^N)(\text{opposite strangeness}) = (\frac{4f_s}{8 + 12f_s}, 0). \quad (63)$

5.  $\nu$ =(two mesons with same strangeness),  
 $(P^A, P^N)(\text{same strangeness}) = (0, 0), \quad (64)$

which is true only to order  $f_s$ . The probabilities will be non-vanishing to the next order of  $f_s^2$ .

6.  $\nu$ =(one  $|S|=1$  meson and one non-strange meson),  
 $(P^A, P^N)(\text{one strange, one non-strange})$   
 $= (\frac{8f_s}{8 + 12f_s}, \frac{32f_s}{16 + 32f_s}). \quad (65)$

### IX. NUMERICAL EXAMPLES OF THEORETICAL $dN/d\Delta\phi d\Delta\eta$ IN FLUX TUBE FRAGMENTATION

Using Eqs. (44), (46), and (53), we obtain the correlation function for two mesons in a charge or strangeness configuration  $\nu$  as given by

$$\begin{aligned} \frac{dN(\nu)}{d\Delta\phi d\Delta\eta} &= P^A(\nu) \frac{1}{1 + e^{(|\Delta\eta| - w)/a}} \frac{dN_T^A}{d\Delta\phi} \\ &+ P^N(\nu) \frac{1}{1 + e^{(w - |\Delta\eta|)/a}} \frac{1}{8\pi^2}, \end{aligned} \quad (66)$$

where  $dN_T^A/d\Delta\phi$  is given by Eq. (38) and its numerical values are shown in Fig. 4.

In typical experimental measurements of the two-hadron angular correlations such as those in the NA61/SHINE Collaboration [46–49], one collects the data for a set of events with similar characteristics (such as charge multiplicities) and picks a pair of mesons of configuration  $\nu$  (for example, of opposite charges) from the same event to build up the “sibling” distribution  $dN_{\text{sib}}(\nu)/d\Delta\phi d\Delta\eta$  per meson pair, as a function of  $\Delta\phi$  and  $\Delta\eta$ . To eliminate systematic errors and to account for the phase space boundaries of the detectors, one also uses this set of data to pick a pair of mesons of configuration  $\nu$  from two different events (mixed events) to build up the “mixed” distribution  $dN_{\text{mix}}(\nu)/d\Delta\phi d\Delta\eta$  per meson pair as a function of  $\Delta\phi$  and  $\Delta\eta$ . The sibling distribution contains all the correlation information while the meson pair from different “mixed” events do not contain any correlation. We can construct the sibling-to-mixed ratio

$$\frac{dN_{\text{sib}}(\nu)/d\Delta\phi d\Delta\eta}{dN_{\text{mix}}(\nu)/d\Delta\phi d\Delta\eta}, \quad (67)$$

which can be compared with theoretical predictions  $C(\Delta\phi, \Delta\eta)$  for such a ratio.

The numerator of Eq. (67) can be identified with the distribution of Eq. (66). The denominator from different events in an event mixing, can be considered in a hypothetical case if the meson pair of configuration  $\nu$  arises in the absence of all correlations. With the absence of correlations in  $\phi$ , then from Eq. (23)  $dN_\phi/d\Delta\phi = 1/8\pi^2$ , and with the absence of space-time-ordering correlations in  $\eta$ , then  $dN_\eta/d\Delta\eta = dN_\eta^A/d\Delta\eta + dN_\eta^N/d\Delta\eta = 1$ . The distribution  $dN_{\text{mix}}(\nu)/d\Delta\phi d\Delta\eta$  in the absence of all correlations is  $[P^A(\nu) + P^N(\nu)]/8\pi^2$ . It is therefore useful to divide the distribution (66) by the scale  $[P^A(\nu) + P^N(\nu)]/8\pi^2$  to construct the following theoretical angular correlation function for comparison with experimental ratio of Eq. (67)

$$C^{\text{single flux tube}}(\Delta\phi, \Delta\eta) = \frac{\frac{dN(\nu)}{d\Delta\phi d\Delta\eta}}{[P^A(\nu) + P^N(\nu)] \frac{1}{8\pi^2}}, \quad (68)$$

where  $dN(\nu)/d\Delta\phi d\Delta\eta$  is given by Eq. (66).

It is however necessary to make an amendment in the above equation in order to compare with the flux tube

fragmentation in  $pp$  collisions. The above result gives theoretical correlation function for a single flux tube. In flux tube fragmentation in  $pp$  collisions, two flux tubes are formed by the diquark of one nucleon forming a flux tube with the valence quark of the other nucleon, and vice-versa. The mesons from one flux tube fragmentation will not be correlated with the mesons from the other flux tube fragmentation, but they are included in the sibling and mixed distributions in the experimental measurement. These uncorrelated mesons from two different flux tubes contribute  $P^N(\nu)/8\pi^2$  to both the sibling and the mixed distributions. Upon taking into account this contribution from two different flux tubes, the proper theoretical angular correlation function for the charge or strangeness configuration  $\nu$  in  $pp$  collisions is

$$C(\Delta\phi, \Delta\eta) = \frac{\frac{P^A(\nu)}{1 + e^{(|\Delta\eta| - w)/a}} \frac{dN_T^A}{d\Delta\phi} + \frac{P^N(\nu)}{1 + e^{(w - |\Delta\eta|)/a}} \frac{1}{8\pi^2} + \frac{P^N(\nu)}{8\pi^2}}{[P^A(\nu) + P^N(\nu)] \frac{1}{8\pi^2} + P^N(\nu) \frac{1}{8\pi^2}}, \quad (69)$$

which is to be compared with the experimental sibling-to-mixed ratio of Eq. (67).

We can consider an explicit numerical example. For  $pp$  collisions at  $\sqrt{s_{NN}} = 200$  GeV, we have  $dN_{\text{ch}}/d\eta|_{\eta \sim 0} \sim 2.25$  [64–66]. As  $pp$  collisions contains contributions from two quark-diquark strings, and each string produces  $dN_{\text{ch}}/d\eta \sim 1.125$ , we therefore have  $w \sim 0.59$  at  $\sqrt{s} = 200$  GeV.

We can estimate the diffuseness parameter  $a$  from the ratio of the width (represented by the standard deviation  $\sigma_\tau$ ) of the distributions of the pair production proper time to the average pair production proper time  $\langle\tau_{\text{pro}}\rangle$ . Previously in the scatter plot of the pair production proper times in the Lund model (see Fig. 2 of [16]), we find

$$\frac{\sigma_\tau}{\langle\tau_{\text{pro}}\rangle} \sim \frac{1}{2}. \quad (70)$$

From Eqs. (39) and (41),  $w$  is inversely proportional to the pair production proper time  $\tau_{\text{pro}}$ . Hence, we have

$$\frac{(\text{width of } w)}{w} = \frac{(\text{width of } \tau_{\text{pro}})}{\langle\tau_{\text{pro}}\rangle}. \quad (71)$$

The width of  $w$  can be identified with  $1.5a$ , for which the Fermi distribution of Eq. (43) drops from 82% to 0.18% at  $w - 1.5a$  to  $w + 1.5a$ . We obtain then

$$\frac{1.5a}{w} \sim \frac{\sigma_\tau}{\langle\tau_{\text{pro}}\rangle} \sim \frac{1}{2}, \quad \text{and } a \sim 0.2. \quad (72)$$

For numerical purposes, we shall use  $w = 0.59$  and  $a = 0.2$  in subsequent calculations.

#### A. Mesons with Opposite Charges

For the case of a pair of mesons with opposite charges, the probabilities for the pair to be in the adjacent

and non-adjacent states, as given by Eq. (60), are  $(P^A, P^N)=(0.25,0.125)$ .

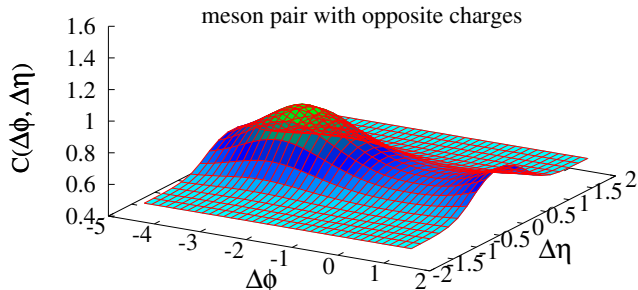


FIG. 6. (Color online) The two-meson angular correlation  $C(\Delta\phi, \Delta\eta)$  for two oppositely charged mesons in a flux tube fragmentation in  $pp$  collisions.

In Fig. 6, the contributions in Eq. (69) combine together to yield the two-meson angular correlation  $C(\Delta\phi, \Delta\eta)$ , in a flux tube fragmentation for two meson with opposite charges, calculated for the sample case of  $w=0.59$  and  $a=0.2$  in  $pp$  collisions. We observe that the correlation is suppressed at  $(\Delta\phi, \Delta\eta) \sim 0$  but is significantly enhanced at  $(\Delta\phi \sim \pi, \Delta\eta \sim 0)$ . Such a correlation arises from the conservation of momentum, charge, and flavor in the production of a quark and an antiquark that become constituents of the two adjacent mesons. For two adjacent mesons that arises from the nearest neighbors, their momenta are likely to be azimuthally correlated to be back-to-back because a constituent of one of the mesons and a constituent of the other meson share the same pair production process at the same spatial point that requires local conservation of momentum. Their charges are likely to have opposite signs because the constituent of one of the mesons and the constituent of the other meson share the same pair production process that requires local charge conservation.

### B. Mesons with Charges of the Same Sign

For the measurement on a pair of mesons with charges of the same sign, the probabilities for the pair to be in the adjacent and non-adjacent states, as given by Eq. (61), are  $(P^A, P^N)=(0,0.125)$ . Because  $P^A = 0$ , the correlation is independent of  $\Delta\phi$ .

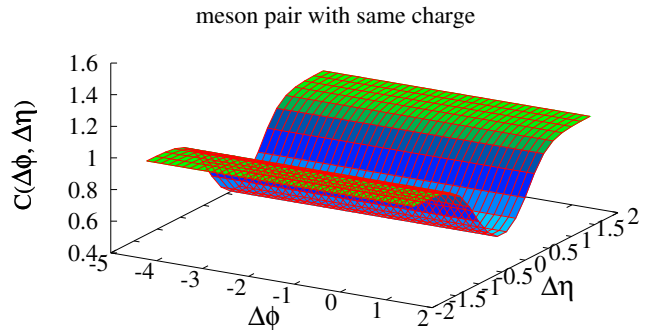


FIG. 7. (Color online) The two-meson angular correlation  $C(\Delta\phi, \Delta\eta)$  for meson pairs with charges of the same sign in a flux tube fragmentation in  $pp$  collisions.

We show in Fig. 7 the correlation function  $C(\Delta\phi, \Delta\eta)$  in a flux tube fragmentation for a pair of mesons with charges of the same sign. We observe a suppression at  $\Delta\eta \sim 0$  indicating that few, if any, pairs of mesons can be produced with charges of the same sign at  $\Delta\eta \sim 0$ . Such a suppression arises because  $\Delta\eta \sim 0$  signals the meson to be adjacently produced but mesons produced adjacently are forbidden to have charges of the same sign, as indicated in Table VI.

### C. Charged Meson Pair

In another example of charge combinations, one detects a pair of charged mesons and measures the correlation between one charged meson with another charged meson. Then from Eq. (62), we have  $(P^A, P^N)=(0.25,0.25)$ . There is an equal probability for the two mesons to be an adjacent pair or a non-adjacent pair.

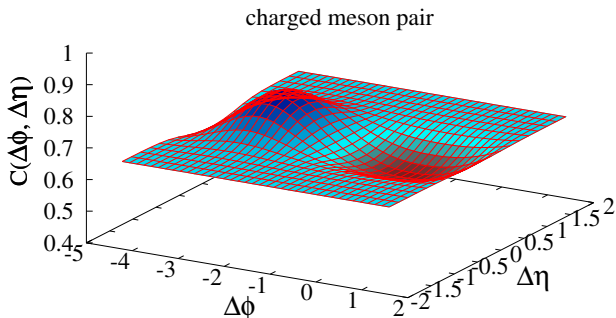


FIG. 8. (Color online) The two-meson angular correlation  $C(\Delta\phi, \Delta\eta)$  for charged meson pairs in a flux tube fragmentation in  $pp$  collisions.

We show the two-meson angular correlation  $C(\Delta\phi, \Delta\eta)$  for two charged mesons for the case of flux tube fragmentation in Fig. 8. It is in fact related to the sum of the correlation functions of Figs. 6 and 7. The suppression at  $(\Delta\phi, \Delta\eta) \sim 0$  arises from the suppression of charges both of the same sign and opposite signs at  $(\Delta\phi, \Delta\eta) \sim 0$ , while the enhancement at  $(\Delta\phi \sim \pi, \Delta\eta \sim 0)$  arises from the back-to-back enhanced correlation of charges of opposite signs in adjacent mesons.

#### D. Mesons with Opposite Strangeness

For a pair of mesons with opposite strangeness, Eq. (63) gives the probability  $P^A = f_s/(2 + 3f_s)$  for the pair to be in the adjacent state. The probability  $P^N$  is zero, up to the first order in  $f_s$ . It becomes non-zero only when we include contributions up to the next higher order terms in  $f_s^2$ .

As an example, we examine the case for  $pp$  collisions at  $\sqrt{s_{NN}} = 200$  GeV for which  $f_s = 0.1$ , as given in Appendix A. Eqs. (63) then gives  $(P^A, P^N) = (0.043, 0)$ . We show in Fig. 9 the correlation function for two mesons with opposite strangeness quantum numbers. The correlation pattern of such a case is quite distinct. It is suppressed at  $(\Delta\phi, \Delta\eta) \sim 0$  and enhanced at  $(\Delta\phi \sim \pi, \Delta\eta \sim 0)$ . As one notes from Eq. (69), because  $P^N$  is zero, the distribution  $C(\Delta\phi, \Delta\eta)$  for this case is independent of  $f_s$ .

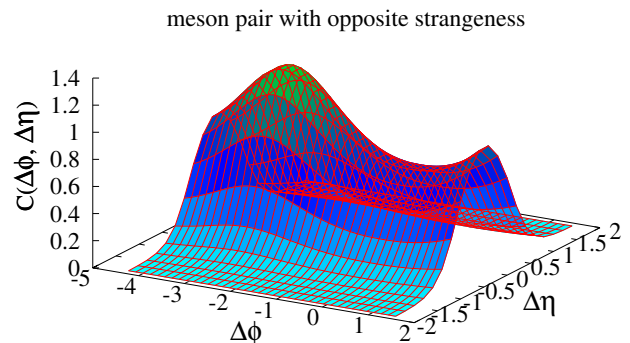


FIG. 9. (Color online) The two-meson angular correlation  $C(\Delta\phi, \Delta\eta)$  for two mesons with opposite strangeness in a flux tube fragmentation in  $pp$  collisions.

#### E. Production of Mesons with Other Strangeness Configurations

For the case of two mesons with the same non-zero strangeness, the probabilities for adjacent and non-adjacent mesons is zero up to order  $f_s$ . They are non-zero only when we include additional contributions from the higher order of order  $f_s^2$ .

From Eq. (65), the case of the correlation of one meson with strangeness  $|S|=1$  and another non-strange meson with  $S=0$  gives  $(P^A, P^N) = (0.086, 0.167)$ . We show the correlation function in Fig. 10 which has a shape that is different from other configurations.

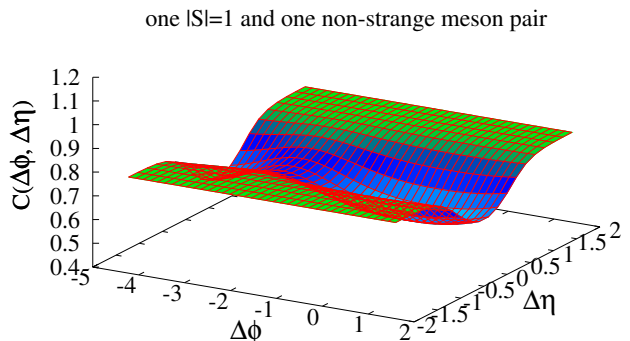


FIG. 10. (Color online) The two-meson angular correlation  $C(\Delta\phi, \Delta\eta)$  for one meson with strangeness  $|S|=1$  and another non-strange meson with  $S=0$  in a flux tube fragmentation in  $pp$  collisions.



## X. COMPARISON WITH EXPERIMENT

In a  $pp$  high-energy collision, most of the produced mesons are pions, with some fractions of strange particles and higher resonances. The strangeness fraction is indicated by the  $K^+/\pi^+$  ratio that depends on the collision energy. It is of order 0.1 at  $\sqrt{s_{NN}}=200$  GeV and it decreases as the collision energy decreases [46–49, 64–67]. The resonance fraction, relative to the number of pion, is of order  $\exp\{-(m_{\text{resonance}} - m_\pi)/T_{\text{eff}}\}$ , and it increases with increasing collision energy. For an effective temperature of order 200 to 300 MeV for  $pp$  collisions at  $\sqrt{s_{NN}}\sim 6\text{--}200$  GeV, the resonance fraction for  $\rho$  or  $\omega$  mesons is of order  $e^{-3}$  to  $e^{-2}$ , or 5 to 14 percent. A resonance fraction of such an amount would modify  $P^A$  and  $P^N$  by about 10 to 15% and would not change greatly the gross features of the two-hadron correlation patterns in flux tube fragmentation shown in the last section.

### A. Comparison with STAR Two-Hadron Correlation Data at $\sqrt{s_{NN}}=200$ GeV

The Star Collaboration measured the angular correlation of produced charged hadrons represented by  $\Delta\rho/\sqrt{\rho_{\text{ref}}}$  which is related to the correlation function  $C(\Delta\phi, \Delta\eta)$  of Eq. (69) by

$$\frac{\Delta\rho}{\sqrt{\rho_{\text{ref}}}} = \rho_0 \left\{ \frac{\Delta\rho}{\rho_{\text{ref}}} - 1 \right\} = \rho_0 \{C(\Delta\phi, \Delta\eta) - 1\}, \quad (73)$$

where  $\Delta\rho = \rho - \rho_{\text{ref}}$ ,  $\rho$  is the correlated distribution from sibling events,  $\rho_{\text{ref}}$  is the reference distribution from mixed events, and  $\rho_0 \approx \sqrt{\rho_{\text{ref}}}$  is the 2D angular density averaged over the angular acceptance  $(\Delta\phi, \Delta\eta)$  [41–45]. Thus,  $C(\Delta\phi, \Delta\eta)$  has the same shape as  $\Delta\rho/\sqrt{\rho_{\text{ref}}}$  and differs by an overall constant factor and an off-set.

The Star Collaboration found that if one separates the transverse momentum regions by the boundary  $p_{Tb}=0.5$  GeV/c, the correlation  $\Delta\rho/\sqrt{\rho_{\text{ref}}}$  for two oppositely-charged mesons in the domain below  $p_T < p_{Tb}$ , as shown in Fig. I(a), is distinctly different from the correlation pattern in the domain above  $p_T > p_{Tb}$ , as shown in Fig. I(b). We mentioned earlier in the Introduction that the two hadron correlation pattern of Fig. I(b) is a signature of the hard-scattering process, with the occurrence of a jet (minijet) at  $(\Delta\phi, \Delta\eta) \sim 0$ , and another back-to-back jet at the away side with a ridge at  $\Delta\phi \sim \pi$ .

In Fig. I(a) the small narrow peak at  $(\Delta\phi, \Delta\eta) \sim 0$  arises from  $e^+e^-$  pairs produced by photon conversion in the detector and is an experimental artifact. After removing the narrow sharp peak at  $(\Delta\phi, \Delta\eta) \sim 0$  from our consideration, we find that the theoretical correlation pattern for two oppositely charged hadrons shown in Fig. 6 for flux tube fragmentation has the same gross features as the experimental correlation pattern obtained by the STAR Collaboration in Fig. I(a), for two oppositely-charged hadrons with  $p_T < 0.5$  GeV/c in  $pp$  collisions at  $\sqrt{s_{NN}}=200$  GeV. There is a depression at  $(\Delta\eta, \Delta\phi) \sim 0$

but an enhancement at  $(\Delta\eta \sim 0, \Delta\phi \sim \pi)$ . The similarity in the gross features in Figs. I(a) and Fig. 6 indicates that in the domain with  $p_T < 0.5$  GeV/c, the dominant particle production mechanism is qualitatively consistent with the flux tube fragmentation mechanism. Our theoretical result from a microscopic approach supports the earlier suggestion by the STAR collaboration [41–45] to use the two-hadron correlation of opposite charges as the signature for the soft particle production process, and we identify this soft process as flux tube fragmentation.

There are other signatures of the flux tube fragmentation for mesons with charges of the same signs, or for all charged meson pairs. The comparison is complicated by the presence of Bose-Einstein correlations for identical bosons. Such a two-body Bose-Einstein correlation is an enhanced correlation at  $(\Delta\phi, \Delta\eta) \sim 0$  and it masks the large suppression of the correlation arising from flux tube fragmentation. For the correlation of hadron pairs with charges of the same sign or for all charged meson pairs, it is however necessary to subtract the contribution from Bose-Einstein correlations of identical bosons before one can make a meaningful comparison. For direct comparisons, correlation of hadrons with opposite charges or opposite strangeness may provide the best tools as signatures for flux tube fragmentation.

### B. Comparison with NA61/SHINE Two-Hadron Correlation Data at $\sqrt{s_{NN}}=6\text{--}17$ GeV

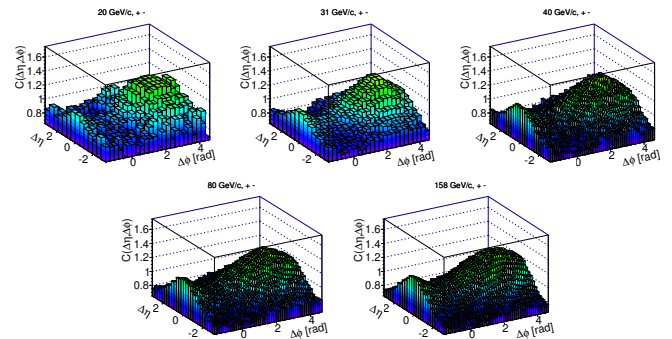


FIG. 11. (Color online) NA61/SHINE two-hadron correlation data  $C(\Delta\eta, \Delta\phi)$  [46–49] for two hadrons of opposite charges with  $p_T < 1.5$  GeV/c, for  $pp$  collisions at different energies (from Fig. 3 of Ref. [46]). From left to right and from top to bottom, the collision energies are  $\sqrt{s_{NN}} = 6.3, 7.6, 8.7, 12.3, 17.2$  GeV.

The NA61/SHINE Collaboration has reported the angular correlation  $C(\Delta\eta, \Delta\phi) \propto dN/d\Delta\phi d\Delta\eta$  for two hadrons with opposite charges and  $p_T < 1.5$  GeV/c, for  $pp$  collisions at  $\sqrt{s_{NN}}=6\text{--}17$  GeV shown in Fig. 11 [46–49]. One can make the following remarks:

1. The experimental correlation patterns for two hadrons with opposite charges in Fig. 11 have the same gross features as the signature for the flux



tube fragmentation shown in Fig. 6, indicating that the dominant mechanism of particle production for  $p_T$  hadrons in the domain with  $p_T < 1.5$  GeV/c is qualitatively consistent with the flux tube fragmentation. The pattern of the NA61/SHINE two-hadron correlation was also shown to be qualitatively consistent with the EPOS model [46, 68]. Although there are many different processes and diagrams in the EPOS model, it is likely that the dominant process responsible for such a two-hadron correlation pattern is the flux tube fragmentation part of the EPOS model.

2. According to Eq. (44), the width in the  $\Delta\eta$  direction is inversely proportional to  $dN/d\eta|_{\eta \sim 0}$ . Thus, as the energy decreases,  $dN/d\eta|_{\eta \sim 0}$  decreases, and one expects the width in  $\Delta\eta$  to increase. There is a hint of such an increase of the  $\Delta\eta$  width in the data of Fig. 11 but a more accurate determination of the  $\Delta\eta$  width will be needed.
3. The correlation pattern of Fig. 11 remains unchanged by shifting the  $p_T$  domain up to  $p_T = 1.5$  GeV/c [46]. This means that in the collision energy range of  $\sqrt{s_{NN}} = 6$  to 17 GeV, the domain boundary  $p_{Tb}$  between the flux tube fragmentation process and the hard-scattering process is greater than 1.5 GeV/c. The boundary  $p_{Tb}$  can be located by searching for a change of the two-hadron correlation pattern for oppositely charged hadrons from that of the flux tube fragmentation process of Fig. I(a) and Fig. 6 to that of the hard scattering process of Fig. I(b), as  $p_{Tb}$  increases beyond 1.5 GeV/c.

For  $\sqrt{s_{NN}} = 200$  GeV, the transverse momentum boundary has been located at  $p_{Tb} = 0.5$  GeV/c [42]. This shows that as the collision energy increases, the fractional contributions from the hard-scattering process increases, and the boundary  $p_{Tb}$  has been found to move from  $p_{Tb}$  greater than 1.5 GeV/c for  $\sqrt{s_{NN}} = 6-17$  GeV [46] to the lower value of  $p_{Tb} = 0.5$  GeV/c for  $\sqrt{s_{NN}} = 200$  GeV [42]. The search for the boundary  $p_{Tb}$  in an energy scan will map out  $p_{Tb}(\sqrt{s_{NN}})$  more precisely as a decreasing function of the  $pp$  collision energy  $\sqrt{s_{NN}}$ .

4. There are additional predicted correlations of two hadrons with opposite strangeness and the correlation of a strange meson with a non-strange meson, as shown in Figs. 9 and 10 where the two-hadron correlation patterns for flux tube fragmentation are quite distinct and may be tested with the NA61/SHINE experimental measurements.
5. In  $pp$  collisions at NA61/SHINE energies, baryon resonances can be produced by exciting the incident projectile and target protons. The decays of these baryon resonances will lead to a greater numbers of  $\pi^+$  as compared to  $\pi^-$  and are likely to occur in the projectile and target fragmentation regions

with a diminishing influence in the central rapidity region. At central rapidity, contributions of  $\pi^+$  from baryon decay has been estimated to be about 20% at  $\sqrt{s_{NN}} = 6$  GeV and it decreases rapidly as a function of collision energies [67]. Correlations of two hadrons with charges of opposite signs as shown in Fig. 11 are likely to receive a greater contribution from the fragmentation of a flux tube than from the decay of baryon resonances.

## XI. SUMMARY AND CONCLUSIONS

The fragmentation of a flux tube is initiated by the production of quark-antiquark pairs along the tube. The production of the  $q\bar{q}$  pairs occurs locally. By the property of local conservation laws, a quark and an antiquark produced at the same point must balance momentum, charge, and flavor. Subsequent to its production, a member of the produced  $q\bar{q}$  pair interacts with its neighboring antiparticles to form a detected meson. Local conservation laws will lead to correlations of the adjacently produced mesons. On the other hand, the production of mesons along a flux tube is ordered in space-time and rapidity. Mesons that are produced adjacent to each other are also close in rapidity. Hence, the proximity of rapidity with a rapidity difference  $\Delta y$  (or approximately a pseudorapidity difference  $\Delta\eta$ ) closer than a rapidity width  $w = 1/(dN/dy)$  can signal their adjacent origin from flux tube fragmentation and the correlation in momentum, charge, and flavor. Using the rapidity ordering as a signal for producing adjacent mesons, we find that  $dN/d\Delta\phi d\Delta\eta$  correlation probability or equivalently  $C(\Delta\phi, \Delta\eta)$  for two opposite charges or strangeness mesons is suppressed on the near-side at  $(\Delta\phi, \Delta\eta) \sim 0$  but the correlation probability is enhanced on the away side at  $(\Delta\phi \sim \pi, \Delta\eta \sim 0)$ .

In addition to flux tube fragmentation, there is the hard-scattering process in nucleon-nucleon collisions. The correlation patterns of hard-scattering is well known, with a peak correlation at  $(\Delta\phi, \Delta\eta) \sim 0$  on the near-side and a ridge along the  $\Delta\eta$  direction at  $\Delta\phi \sim \pi$  on the away side. The use of the signatures for flux tube fragmentation and hard scattering allows one to separate out the dominance of each process in different  $p_T$  domains separated by the domain boundary  $p_{Tb}$ .

In our comparison of the theoretical results with experimental data, we find that the gross features of the signature of flux tube fragmentation for two oppositely charged hadrons are similar to those of the STAR [41–45] and NA61/SHINE [46–49] angular correlation data for two hadrons with opposite charges in the low  $p_T$  region, indicating that the dominant particle production mechanism for low  $p_T$  particles is qualitatively consistent with flux tube fragmentation.

We note that whereas the boundary  $p_{Tb}$  that separates the flux tube fragmentation from the hard-scattering processes in  $pp$  collisions lies beyond  $p_{Tb} > 1.5$  GeV/c

at the NA61/SHINE collision energies of  $\sqrt{s_{NN}}=6-17$  GeV, it shifts to  $p_{Tb}=0.5$  GeV/c at the RHIC energy of  $\sqrt{s_{NN}}=200$  GeV. Thus, the boundary  $p_{Tb}$  has been observed to shift to a lower value of  $p_{Tb}$  as the collision energy increases. Future determination of  $p_{Tb}$  in the energy scan of NA61/SHINE will map out the boundary function  $p_{Tb}(\sqrt{s_{NN}})$  as a precise function of the collision energy  $\sqrt{s_{NN}}$ . In addition to being an intrinsic physical property of the  $pp$  collision process, the boundary function  $p_{Tb}(\sqrt{s_{NN}})$  separating the two processes in  $pp$  collisions also may have implications on the early evolution and thermalization of particles, the quenching of jets, and the formation of the quark-gluon plasma, in high-energy nucleus-nucleus collisions.

Returning to the decomposition of particle production mechanisms into soft and hard components in  $pp$  collisions, our theoretical result from a microscopic approach of the flux tube fragmentation supports the earlier phenomenological suggestion by the STAR Collaboration in [41–45] to associate the correlation of two hadrons with opposite charges to the dominance of the soft component of particle production in the domain with  $p_T < 0.5$  GeV/c. However, our result from a microscopic approach does not support the second phenomenological suggestion in [41–45] of a one-dimensional Gaussian of  $\Delta\eta$  independent of  $\Delta\phi$ . For a better accuracy, a distribution such as Eq. (44) would be a better representation of the two-hadron correlation function of the ‘soft’ component for hadrons with opposite charges than a one-dimensional Gaussian.

The interference of the Bose-Einstein correlation makes it difficult to use the correlations of two hadron of the same sign or two charged hadrons as signatures of the flux tube fragmentation process. In addition to the Bose-Einstein correlation of identical bosons, there is also the production of resonances that will complicate the pattern of two-hadron correlations. The untangling of these many different correlations patterns as a function of collision energies will provide more precise information on the changing role of the flux-tube fragmentation and hard scattering as a function of the collision energy.

Our successes in identifying the signature of the fragmentation of a flux tube will provide a window to examine further the dynamics of the many-pion system and the associated many-pion correlations produced in the flux tube fragmentation. The space-time-rapidity ordering stipulates a very simple many-meson space-time-rapidity correlations. One may wish to find out how a chain of many mesons correlate with each other in their azimuthal angles and rapidities, after their production in a flux tube fragmentation. An interesting experimental and theoretical question is the case of an exclusive measurement on an event-by-event basis if the momenta of all mesons in the flux tube fragmentation have been measured, whether it is possible to piece together different produced mesons in that event to come up with the configuration of the whole system at the moment of its fragmentation. These and many other questions may be opened up for examination upon a successful experimen-

tal search for the signature of the flux tube fragmentation.

### Appendix A: Relation between $K^+/\pi^+$ ratio and $f_s$

In  $pp$  collisions at  $\sqrt{s_{NN}} \sim 6-17$  GeV, the ratios  $K^+/\pi^+$ ,  $K^-/\pi^-$ , and  $\pi^+/\pi^-$  depend on the collision energy and are affected by the rescattering and decays of baryonic resonances formed by the inelastic scattering of the incident protons. As a consequence, the ratio  $K^+/\pi^+$  is greater than  $K^-/\pi^-$  [46–48, 67]. In higher energy  $pp$  collisions at  $\sqrt{s_{NN}}=200$  GeV, the effects of rescattering and the decays of baryonic resonances are less important in the central rapidity region, and  $K^+/\pi^+ \sim K^-/\pi^- \sim 0.10-0.12$ , and  $\pi^+/\pi^- \sim 1$  [64]. It becomes appropriate to estimate the strangeness suppression factor  $f_s$  at  $\sqrt{s_{NN}}=200$  GeV using the flux tube fragmentation model. In such a model, Table V gives the number of cases  $N^{A(ud,s)}(Q_{12}, Q_{34})$  with meson charges  $(Q_{12}, Q_{34})$  in various charge states in the non-strange sector, and the strange sector, for a pair of adjacent mesons. We can treat the pair production at all other vertices as a copy of Table V, which can then be used to calculate the ratio of the single particle production of  $\pi^+$  and  $K^+$ . We find from Table V the number of cases of non-strange ( $u\bar{d}$ ) mesons with a positive charge,

$$\sum_{Q_{12}, Q_{34}=+1, (u\bar{d})} N^{(ud)}(Q_{12}, Q_{34}) = 4 + 2f_s. \quad (\text{A1})$$

We find from table V the number of cases of strange ( $u\bar{s}$ ) mesons with a positive charge,

$$\sum_{Q_{12}, Q_{34}=+1, (u\bar{s})} N^{(s)}(Q_{12}, Q_{34}) = 4f_s. \quad (\text{A2})$$

Therefore, we have

$$\frac{(\text{number of positive strange } K^+ \text{ meson})}{(\text{number of positive non-strange } \pi^+ \text{ mesons})} \sim \frac{(u\bar{s})}{(u\bar{d})} = \frac{4f_s}{4 + 2f_s}. \quad (\text{A3})$$

Experimentally, at  $\sqrt{s} > 200$  GeV, the STAR Collaboration gives [64]

$$\frac{K^+}{\pi^+} = \frac{(\text{number of } K^+)}{(\text{number of } \pi^+)} = 0.10 \text{ to } 0.12, \quad (\text{A4})$$

which leads to the estimate

$$f_s = 0.105 \text{ to } 0.126. \quad (\text{A5})$$

Although Table V may appear complicated, it is intuitively reasonable that  $K^+/\pi^+$  should be nearly equal to  $f_s$  in flux tube fragmentation because given a  $u$  quark,  $\pi^+$  is the result of a  $d-\bar{d}$  pair production, and  $K^+$  is the result of an  $s-\bar{s}$  pair production with a reduced probability  $f_s$ . Hence,  $K^+/\pi^+$  should be nearly equal to  $f_s$ .

It should be pointed out that the strangeness suppression factor we have estimated is significantly smaller than the value of  $f_s=0.3$  used in the standard Lund Monte Carlo programs [10, 27]. The determination of  $f_s$  in the flux tube fragmentation from the  $K^+/\pi^+$  ratio is best carried out when the flux tube fragmentation process can be isolated without interference from contributions from other mechanisms. However, for  $pp$  collisions at energies much below  $\sqrt{s} = 200$  GeV, the production is influenced by contributions from baryon resonance production in which an incident proton is excited to a baryon resonance which subsequently emit a meson [47, 48]. The baryon resonance are produced mostly at the projectile and target fragmentation regions but have contributions at central rapidity when the collision energies are low as in the  $\sqrt{s} \sim 10$  GeV region. The determination of  $f_s$  in these lower energy region will be affected by the parameters specifying baryon resonance production processes. Only for high enough energies at central rapidity can the flux tube fragmentation processes be isolated with small contributions from baryon resonance contributions. Future extraction of  $f_s$  for the flux tube fragmentation around  $\sqrt{s} = 200$  GeV with  $p_T < 0.5$  GeV/c will be of interest in clarifying the magnitude of the strangeness suppression factor  $f_s$ .

### Appendix B: Charge and Strangeness Configurations for Flux Tube Fragmentation of Two Non-adjacent Mesons with Three Flavors

We examine the quark charge and flavor configurations in two non-adjacent mesons  $P_{12}$  and  $P_{34}$  in flux tube fragmentation with three flavors as depicted in Fig. 3. The constituents  $p_2$  and  $p_3$  are produced at different vertices and are not constrained by charge and flavor conservation. The cases of possible charge and strangeness configurations come in three parts. By including only cases up to the first order in  $f_s$ , we list the charge and strangeness configurations in which  $p_2$  is a  $u$  quark in Table X as Part I,  $p_2$  is a  $d$  quark in Table XIII as Part II, and  $p_2$  is an  $s$  quark in Table XVI as Part III. The corresponding number of cases  $N^{N(ud)}(Q_{12}, Q_{34})$  in the non-strange sector and  $N^{N(s)}(Q_{12}, Q_{34})$  in the strange sector are given in Tables XI, XII, XIV, XV, XVII, and XVIII.

In a flux tube fragmentation with three flavors for non-adjacent mesons  $P_{12}$  and  $P_{34}$  in which  $p_2$  is a  $u$  quark, we can use Table X to construct Table XI as Part I of the number of cases  $N^{N(ud,s)}(Q_{12}, Q_{34})$  in the strange and non-strange sectors.

TABLE X. Part I of quark and antiquark configurations with three flavors for two non-adjacent mesons  $P_{12}$  and  $P_{34}$  in a flux tube fragmentation with three flavors in which  $p_2$  is an  $u$  quark.

$p_1$	$p_2$	$Q_{12}$	$S_{12}$	$p_3$	$p_4$	$Q_{34}$	$S_{34}$	Order
$\bar{u}$	$u$	0	0	$\bar{u}$	$d$	-1	0	1
$\bar{d}$	$u$	1	0	$\bar{u}$	$d$	-1	0	1
$\bar{u}$	$u$	0	0	$\bar{u}$	$u$	0	0	1
$\bar{d}$	$u$	1	0	$\bar{u}$	$u$	0	0	1
$\bar{u}$	$u$	0	0	$\bar{d}$	$d$	0	0	1
$\bar{d}$	$u$	1	0	$\bar{d}$	$d$	0	0	1
$\bar{u}$	$u$	0	0	$\bar{d}$	$u$	1	0	1
$\bar{d}$	$u$	1	0	$\bar{d}$	$u$	1	0	1
$\bar{s}$	$u$	1	1	$\bar{u}$	$d$	-1	0	$f_s$
$\bar{s}$	$u$	1	1	$\bar{u}$	$u$	0	0	$f_s$
$\bar{u}$	$u$	0	0	$\bar{u}$	$s$	-1	-1	$f_s$
$\bar{d}$	$u$	1	0	$\bar{u}$	$s$	-1	-1	$f_s$
$\bar{s}$	$u$	1	1	$\bar{d}$	$d$	0	0	$f_s$
$\bar{s}$	$u$	1	1	$\bar{d}$	$u$	1	0	$f_s$
$\bar{u}$	$u$	0	0	$\bar{d}$	$s$	0	-1	$f_s$
$\bar{d}$	$u$	1	0	$\bar{d}$	$s$	0	-1	$f_s$
$\bar{u}$	$u$	0	0	$\bar{s}$	$d$	0	1	$f_s$
$\bar{d}$	$u$	1	0	$\bar{s}$	$d$	0	1	$f_s$
$\bar{u}$	$u$	0	0	$\bar{s}$	$u$	1	1	$f_s$
$\bar{d}$	$u$	1	0	$\bar{s}$	$u$	1	1	$f_s$

TABLE XI. Part I of the number of cases  $N^{N(ud,s)}(Q_{12}, Q_{34})$  for non-adjacent mesons in different charge states ( $Q_{12}, Q_{34}$ ) in the non-strange sector ( $ud$ ) and the strange sector ( $s$ ), in the fragmentation of a flux tube with three flavors in which  $p_2$  is an  $u$  quark.

		$Q_{34}=-1$	$Q_{34}=0$	$Q_{34}=1$
$N^{N(ud)}(Q_{12}, Q_{34})$	$Q_{12}=-1$	0	0	0
	$Q_{12}=0$	1	2	1
	$Q_{12}=1$	1	2	1
$N^{N(s)}(Q_{12}, Q_{34})$	$Q_{12}=-1$	0	0	0
	$Q_{12}=0$	$f_s$	$2f_s$	$f_s$
	$Q_{12}=1$	$2f_s$	$4f_s$	$2f_s$

From the above Table X we can similarly construct Table XII as Part I of the number of cases  $N^{N(ud,s)}(S_{12}, S_{34})$  for non-adjacent mesons  $P_{12}$  and  $P_{34}$  in different strangeness states ( $S_{12}, S_{34}$ ), in the fragmentation of a flux tube with three flavors in which  $p_2$  is an  $u$  quark.

TABLE XII. Part I of the number of cases  $N^{N(s)}(S_{12}, S_{34})$  for non-adjacent mesons  $P_{12}$  and  $P_{34}$  in different strangeness states ( $S_{12}, S_{34}$ ) in a flux tube fragmentation with three flavors, in which  $p_2$  is an  $u$  quark.

		$S_{34}=-1$	$S_{34}=0$	$S_{34}=1$
$N^{N(s)}(S_{12}, S_{34})$	$S_{12}=-1$	0	0	0
	$S_{12}=0$	$4f_s$	0	$4f_s$
	$S_{12}=1$	0	$4f_s$	0

In a flux tube fragmentation with three flavors for non-

adjacent mesons  $P_{12}$  and  $P_{34}$  in which  $p_2$  is a  $d$  quark, the possible charge and strangeness configurations are listed in Table XIII as Part II.

TABLE XIII. Part II of quark and antiquark configurations with three flavors for two non-adjacent mesons  $P_{12}$  and  $P_{34}$  in a flux tube fragmentation with three flavors in which  $p_2$  is a  $d$  quark.

$p_1$	$p_2$	$Q_{12}$	$s_{12}$	$p_3$	$p_4$	$Q_{34}$	$s_{34}$	Order
$\bar{u}$	$d$	-1	0	$\bar{u}$	$d$	-1	0	1
$\bar{d}$	$d$	0	0	$\bar{u}$	$d$	-1	0	1
$\bar{u}$	$d$	-1	0	$\bar{u}$	$u$	0	0	1
$\bar{d}$	$d$	0	0	$\bar{u}$	$u$	0	0	1
$\bar{u}$	$d$	-1	0	$\bar{d}$	$d$	0	0	1
$\bar{d}$	$d$	0	0	$\bar{d}$	$d$	0	0	1
$\bar{u}$	$d$	-1	0	$\bar{d}$	$u$	1	0	1
$\bar{d}$	$d$	0	0	$\bar{d}$	$u$	1	0	1
$\bar{s}$	$d$	0	1	$\bar{u}$	$d$	-1	0	$f_s$
$\bar{s}$	$d$	0	1	$\bar{u}$	$u$	0	0	$f_s$
$\bar{u}$	$d$	-1	0	$\bar{u}$	$s$	-1	-1	$f_s$
$\bar{d}$	$d$	0	0	$\bar{u}$	$s$	-1	-1	$f_s$
$\bar{s}$	$d$	0	1	$\bar{d}$	$d$	0	0	$f_s$
$\bar{s}$	$d$	0	1	$\bar{d}$	$u$	1	0	$f_s$
$\bar{u}$	$d$	-1	0	$\bar{d}$	$s$	0	-1	$f_s$
$\bar{d}$	$d$	0	0	$\bar{d}$	$s$	0	-1	$f_s$
$\bar{u}$	$d$	-1	0	$\bar{s}$	$d$	0	1	$f_s$
$\bar{d}$	$d$	0	0	$\bar{s}$	$d$	0	1	$f_s$
$\bar{u}$	$d$	-1	0	$\bar{s}$	$u$	1	1	$f_s$
$\bar{d}$	$d$	0	0	$\bar{s}$	$u$	1	1	$f_s$

From the above Table XIII we can construct Table XIV as Part II of the number of cases  $N^{N(ud,s)}(Q_{12}, Q_{34})$  for non-adjacent mesons  $P_{12}$  and  $P_{34}$  to be in different charge states  $(Q_{12}, Q_{34})$  in the non-strange and strange sectors, in a flux tube fragmentation with three flavors in which  $p_2$  is a  $d$  quark.

TABLE XIV. Part II of the number of cases  $N^{N(ud,s)}(Q_{12}, Q_{34})$  for non-adjacent mesons in different charge states  $(Q_{12}, Q_{34})$  in the non-strange sector ( $ud$ ) and the strange sector ( $s$ ), in a flux tube fragmentation with three flavors in which  $p_2$  is a  $d$  quark.

		$Q_{34}=-1$	$Q_{34}=0$	$Q_{34}=1$
$N^{N(ud)}(Q_{12}, Q_{34})$	$Q_{12}=-1$	1	2	1
	$Q_{12}=0$	1	2	1
	$Q_{12}=1$	0	0	0
$N^{N(s)}(Q_{12}, Q_{34})$	$Q_{12}=-1$	$f_s$	$2f_s$	$f_s$
	$Q_{12}=0$	$2f_s$	$4f_s$	$2f_s$
	$Q_{12}=1$	0	0	0

From the above Table XIII we can similarly construct Table XV as Part II of the number of cases  $N^{N(ud,s)}(S_{12}, S_{34})$  for non-adjacent mesons  $P_{12}$  and  $P_{34}$  in different strangeness states  $(S_{12}, S_{34})$ , in a flux tube fragmentation with three flavors in which  $p_2$  is a  $d$  quark.

TABLE XV. Part II of the number of cases  $N^{N(s)}(S_{12}, S_{34})$  for non-adjacent mesons  $P_{12}$  and  $P_{34}$  in different strangeness states  $(S_{12}, S_{34})$ , in a flux tube fragmentation with three flavors in which  $p_2$  is a  $d$  quark.

		$S_{34}=-1$	$S_{34}=0$	$S_{34}=1$
$N^{A(s)}(S_{12}, S_{34})$	$S_{12}=-1$	0	0	0
	$S_{12}=0$	$4f_s$	0	$4f_s$
	$S_{12}=1$	0	$4f_s$	0

In a flux tube fragmentation with three flavors in which  $p_2$  is an  $s$  quark, we list all possible charge and strangeness configurations for non-adjacent mesons  $P_{12}$  and  $P_{34}$  in Table XVI as Part III.

TABLE XVI. Part III of quark and antiquark configurations for two non-adjacent mesons  $P_{12}$  and  $P_{34}$  in a flux tube fragmentation with three flavors in which  $p_2$  is an  $s$  quark.

$p_1$	$p_2$	$Q_{12}$	$S_{12}$	$p_3$	$p_4$	$Q_{34}$	$S_{34}$	Order
$\bar{u}$	$s$	-1	-1	$\bar{u}$	$d$	-1	0	$f_s$
$\bar{d}$	$s$	0	-1	$\bar{u}$	$d$	-1	0	$f_s$
$\bar{u}$	$s$	-1	-1	$\bar{u}$	$u$	0	0	$f_s$
$\bar{d}$	$s$	0	-1	$\bar{u}$	$u$	0	0	$f_s$
$\bar{u}$	$s$	-1	-1	$\bar{d}$	$d$	0	0	$f_s$
$\bar{d}$	$s$	0	-1	$\bar{d}$	$d$	0	0	$f_s$
$\bar{u}$	$s$	-1	-1	$\bar{d}$	$u$	1	0	$f_s$
$\bar{d}$	$s$	0	-1	$\bar{d}$	$u$	1	0	$f_s$

From the above Table XVI we can construct Table XVII as Part III of the number of cases  $N^{N(ud,s)}(Q_{12}, Q_{34})$  for non-adjacent mesons  $P_{12}$  and  $P_{34}$  to be in different charge states  $(Q_{12}, Q_{34})$  in the strange and non-strange sectors, in a flux tube fragmentation with three flavors in which  $p_2$  is an  $s$  quark.

TABLE XVII. Part III of the number of cases  $N^{N(ud,s)}(Q_{12}, Q_{34})$  for non-adjacent mesons in different charge states  $(Q_{12}, Q_{34})$  in the non-strange sector ( $ud$ ) and the strange sector ( $s$ ), in a flux tube fragmentation with three flavors in which  $p_2$  is an  $s$  quark.

		$Q_{34}=-1$	$Q_{34}=0$	$Q_{34}=1$
$N^{N(ud)}(Q_{12}, Q_{34})$	$Q_{12}=-1$	0	0	0
	$Q_{12}=0$	0	0	0
	$Q_{12}=1$	0	0	0
$N^{N(s)}(Q_{12}, Q_{34})$	$Q_{12}=-1$	$f_s$	$2f_s$	$f_s$
	$Q_{12}=0$	$f_s$	$2f_s$	$f_s$
	$Q_{12}=1$	0	0	0

From the above Table XVI we can similarly construct Table XVIII as Part III of the number of cases  $N^{N(ud,s)}(S_{12}, S_{34})$  for non-adjacent mesons  $P_{12}$  and  $P_{34}$  in different strangeness states  $(S_{12}, S_{34})$ , in a flux tube fragmentation with three flavors in which  $p_2$  is an  $s$  quark.

Upon adding the contributions from all contributions from Parts I, II and III, we obtain Tables VIII and IX in

TABLE XVIII. Part III of the number of cases  $N^{N(s)}(S_{12}, S_{34})$  for non-adjacent mesons  $P_{12}$  and  $P_{34}$  in different strangeness states  $(S_{12}, S_{34})$  in a flux tube fragmentation, in a flux tube fragmentation with three flavors in which  $p_2$  is an  $s$  quark.

		$S_{34}=-1$	$S_{34}=0$	$S_{34}=1$
$N^{N(s)}(S_{12}, S_{34})$	$S_{12}=-1$	0	$8f_s$	0
	$S_{12}=0$	0	0	0
	$Q_{12}=1$	0	0	0

Section VII.

### Acknowledgments

The author would like to thank Drs. Elena Kokouline and G. Feofilov for helpful discussions. The research was supported in part by the Division of Nuclear Physics, U.S. Department of Energy under Contract DE-AC05-00OR22725.

- 
- [1] J. Schwinger, Phys. Rev. **82**, 664 (1951).  
[2] J. Schwinger, Phys. Rev. **128**, 2425 (1962).  
[3] Y. Nambu, Lectures at Copenhagen Symposium (1970).  
[4] J. D. Bjorken, Lectures presented at the 1973 Proceedings of the Summer Institute on Particle Physics, edited by Zipt, SLAC-167 (1973).  
[5] A. Casher, J. Kogut, and L. Susskind, Phys. Rev. D **10**, 732 (1974).  
[6] X. Artru and G. Mennessier, Nucl. Phys. B **70**, 93 (1974).  
[7] B. Andersson, G. Gustafson and C. Peterson, Z. Phys. C **1**, 105 (1979); B. Andersson, G. Gustafson and B. Söderberg, Z. Phys. C **20**, 317 (1983).  
[8] A comprehensive review of the application of the Flux Tube Fragmentation Model for nucleon-nucleon and  $e^+e^-$  collisions can be found in B. Andersson, G. Gustafson, G. Ingelman, and T. Sjöstrand, Phys. Rep. **97**, 31 (1983), and X. Artru, Phys. Rep. **97**, 147 (1983).  
[9] B. Andersson, G. Gustafson, and T. Sjöstrand, Zeit. für Phys. C **20**, 317 (1983); T. Sjöstrand and M. Bengtsson, Computer Physics Comm. **43**, 367 (1987); B. Andersson, G. Gustafson, and B. Nilsson-Alqvist, Nucl. Phys. B **281**, 289 (1987).  
[10] T. Sjöstrand *et al.*, *An Introduction to PYTHIA 8.2*, arXiv:1410.3012.  
[11] X. Artru, Z. Phys. C **26**, 83 (1984).  
[12] T. Sjöstrand, Comp. Phys. Comm. **39**, 347 (1986); T. Sjöstrand, and M. Bengtsson, Comp. Phys. Comm. **43**, 367 (1987).  
[13] R. C. Wang and C. Y. Wong, Phys. Rev. D **38**, 2890 (1988).  
[14] H-P. Pavel and D. Brink, Zeit. Phys. C **51**, 119 (1991).  
[15] C. Y. Wong, R. C. Wang, and C. C. Shih, Phys. Rev. D **44**, 257 (1991).  
[16] C. Y. Wong, R. C. Wang, Phys. Rev. D **44**, 679 (1991).  
[17] G. Gatoff and C.Y. Wong, Phys. Rev. D **46**, 997 (1992); and C.Y. Wong and G. Gatoff, Phys. Rep. **242**, 1994, 489 (1994).  
[18] C. Y. Wong, R.C Wang, and J.S. Wu, Phys. Rev D **51**, 3940 (1995).  
[19] D.A. Derkach, G.A. Feofilov, Phys. Atom. Nucl. **71**, 2087 (2008); E.O. Bodnya, V.N. Kovalenko, A.M. Puchkov, G.A. Feofilov, AIP Conf.Proc. **1606**, 273 (2014); Adam, Jaroslav *et al.*) JHEP **1505** (2015); G. Feofilov, I. Altsybeev, O. Kochebina, XXII International Baldin Seminar on High Energy Physics Problems 15-20 September, 2014 JINR, Dubna, Russia, PoS(Baldin ISHEPP XXII) 067.  
[20] C. Y. Wong, *Introduction to High-Energy Heavy-Ion Collisions*, World Scientific Publisher, 1994.  
[21] R. Blankenbecler and S. J. Brodsky, Phys. Rev. D **10**, 2973 (1974); R. Blankenbecler, S. J. Brodsky and J. Gunion, Phys. Rev. D **12**, 3469 (1975); E. A. Schmidt and R. Blankenbecler, Phys. Rev. D **15**, 332 (1977).  
[22] A.L.S. Angelis *et al.* (CCOR Collaboration), Phys. Lett. B **79**, 505 (1978).  
[23] A.L.S. Angelis *et al.*, (CCOR Collaboration), Physica Scripta **19**, 116 (1979); A.L.S. Angelis *et al.*, (CCOR Collaboration), Phys. Lett. **B97**, 163 (1980).  
[24] R. P. Feynman, R. D. Field and G. C. Fox, Phys. Rev. D **18**, 3320 (1978).  
[25] J. F. Owens, E. Reya, and M. Glök, Phys. Rev. D **18**, 1501 (1978).  
[26] D. W. Duke, J. F. Owens, Phys. Rev. D **30**, 49 (1984).  
[27] T. Sjöstrand and M. van Zijl, Phys. Rev. D **36**, 2019 (1987); R. Corke and T. Sjöstrand, JHEP **1103**, 032 (2011); T. Sjöstrand and P. Z. Skands, Eur. Phys. J. C **39**, 129 (2005); T. Sjöstrand and P. Z. Skands, JHEP **03**, 053 (2004).  
[28] C. Albajar *et al.* (UA1 Collaboration), Nucl. Phys. B **309**, 405 (1988).  
[29] X.N. Wang and M. Gyulassy, Phys. Rev. D **44**, 3501 (1991) and Phys. Rev. D **45**, 734 (1992).  
[30] J. Rak and M. J. Tannenbaum, *High-pr Physics in the Heavy Ion*, Cambridge University Press, Cambridge, 2013.  
[31] F. Arleo, S. Brodsky, D. S. Hwang and A. M. Sickles, Phys. Rev. Lett. **105**, 062002 (2010).  
[32] C. Y. Wong and G. Wilk, Acta Phys. Pol. B **43**, 2047 (2012).  
[33] C. Y. Wong and G. Wilk, Phys. Rev. D **87**, 114007 (2013).  
[34] C. Y. Wong, G. Wilk, arXiv:1309.7330.  
[35] C. Y. Wong, G. Wilk, L. J. L. Cirto and C. Tsallis; EPJ Web of Conf. **90**, 04002 (2015), arXiv:1412.0474.  
[36] L. J. L. Cirto, C. Tsallis, C.-Y. Wong and G. Wilk, arXiv:1409.3278.  
[37] C. Tsallis, J. Stat. Phys. **52**, 479 (1988) and Eur. Phys. J. A **40**, 257 (2009); M. Gell-Mann and C. Tsallis eds., *Nonextensive Entropy – Interdisciplinary Applications* (Oxford University Press, New York, 2004).  
[38] C. Y. Wong, G. Wilk, L. J. L. Cirto and C. Tsallis, Phys. Rev. D **91**, 114027 (2015).  
[39] R. Hagedorn, Riv. Nuovo Cimento **6**, 1 (1984).  
[40] C. Michael and L. Vanryckeghem, J. Phys. G **3**, L151 (1977); C. Michael, Prog. Part. Nucl. Phys. **2**, 1 (1979).  
[41] J. Adams *et al.* (STAR Collaboration), Phys. Rev. C **74**, 032006 (2006).  
[42] R. J. Porter and T. A. Trainor, (STAR Collaboration), J. Phys. Conf. Ser. **27**, 98 (2005).

- [43] T. A. Trainor and R. L. Ray, Phys. Rev. C **84**, 034906 (2011).
- [44] R. L. Ray, Phys. Rev. D **84**, 034020 (2011); T. A. Trainor and D. J. Prindle, *Improved isolation of the  $p$ - $p$  underlying event based on minimum-bias trigger-associated hadron correlations*, arXiv:1310.0408 [hep-ph].
- [45] T. A. Trainor and D. T. Kettler, Phys. Rev. **C84**, 024910 (2011), arXiv:1010.3048.
- [46] M. Maksiak (NA61/SHINE Collaboration), arXiv:1503.02470.
- [47] M. Gazdzicki (NA61/SHINE Collaboration), EPJ Web Conf. **95**, 01005 (2015), arxiv:1412.4243.
- [48] D. T. Larsen (NA61/SHINE Collaboration), Proceedings of International Conference on Strange Quark Matter, Dubna, July 6-11, 2015 (to be published).
- [49] Andrey Seryakov (NA61/SHINE Collaboration), Proceedings of International Conference on Strange Quark Matter, Dubna, July 6-11, 2015 (to be published).
- [50] M. E. Peskin, Nucl. Phys. **B156**, 365 (1979); G. Bhanot and M. E. Peskin, Nucl. Phys. **B156**, 391 (1979).
- [51] F. J. Yndurain, *Low Energy Pion Physics*, arXiv:hep-ph/0212282.
- [52] C. Y. Wong, Phys. Rev. **C69**, 055202 (2004).
- [53] C. Y. Wong and H. W. Crater, Phys. Rev. **C63**, 044907 (2001).
- [54] P.A.M. Dirac, Canad. J. Math. **2**, 129 (1950); Proc. Roy. Soc. Sect. A **246**, 326 (1958); *Lectures on Quantum Mechanics* (Yeshiva University, Hew York, 1964).
- [55] P. Van Alstine and H.W. Crater, J. Math. Phys. **23**, 1997 (1982); H. W. Crater and P. Van Alstine, Ann. Phys. (N.Y.) **148**, 57 (1983).
- [56] H. W. Crater and P. Van Alstine, Phys. Rev. D1 **37**, 1982 (1988).
- [57] H. Sazdjian, Ann. Phys. **191**, 52 (1989); Phys. Rev. D **33**, 3401 (1986).
- [58] H. W. Crater, R. Becker, Cheuk-Yin Wong, and P. Van Alstine, Phys. Rev. **D46**, 5117 (1992).
- [59] H. W. Crater, C. W. Wong, and C. Y. Wong, Intl. J. Mod. Phys.-E **5**, 589 (1996); J. Mourad and H. Sazdjian, J. Phys. G **21** 267, (1995).
- [60] H. W. Crater, P. Van Alstine Phys. Rev. **D70**, 034026 (2004).
- [61] H. W. Crater, J. H. Yoon, and C. Y. Wong Phys. Rev. **D79**, 034011 (2009).
- [62] T. Barnes and E. S. Swanson, Phys. Rev. **D46**, 131 (1992).
- [63] C. Y. Wong, E. S. Swanson, and T. Barnes, Phys. Rev. **C65**, 014903 (2002).
- [64] J. Adams et al. (STAR Collaboration) Phys. Rev. Lett. **92**, 112301 (2004).
- [65] G. Wolschin, <http://arxiv.org/pdf/1106.3636.pdf> EPL **95**, 61001 (2011), (arxiv:1106.3636).
- [66] B. Alver,(PHOBOS Collaboration), Phys. Rev. **C83**, 024913 (2011).
- [67] V. Yu. Vovchenko, D. V. Anchishkin, and M. I. Gorenstein, Phys. Rev. **C 90**, 024916 (2014); V. Uzhinsky , arXiv:1404.2026.
- [68] K. Werner, F. M. Liu and T. Pierog, Phys. Rev. **C 74**, 044902 (2006). [hep-ph/0506232].